UNIVERSITÀ DEGLI STUDI DI SIENA

Research Doctoral School in

Biochemistry and Molecular Biology - BiBiM 2.0

Cycle: XXXV

Smart nanoparticles for the treatment of ocular degenerative diseases

Supervisors

Professor Luciana Dente

Professor Vittoria Raffa

Ph.D. candidate

Patrizia Colucci

Patrizia Colucci

Firmato digitalmente da Patrizia Colucci
Data: 2023.05.29 13:38:51 +01'00'

2019 – 2022

TABLE OF CONTENT

ABSTRACT

Retinal degeneration refers to the pathological conditions affecting the ocular posterior segment, including age-related macular degeneration, glaucoma, retinopathies and inherited retinal diseases. This pathological process represents the leading cause of partial or complete blindness, which stands as an extremely debilitating condition. At the end of 2019, it has been estimated that at least 2.2 billion people suffering from vision deficit or loss and this number is dramatically set to increase. Among the several endogenous and exogenous stress stimuli have been identified as factors contributing to retinal degeneration, the oxidative stress plays a key role in the pathogenesis of these diseases. Currently, no treatment is available to restore vision and the lack of effective therapeutical options is related to difficulties in targeting the ocular posterior segment and preventing the rapid degradation and clearance of delivered drugs.

The present Ph.D. thesis focused on the development of a nanomedicine-based approach for delivering neuroprotective drugs to the posterior segment of the eye as a strategy to counteract retinal dysfunction. Particularly, we synthesised an organic polymer-based nanoformulation (ANPs), which was functionalised with peanut agglutinin (PNA) and nerve growth factor (NGF). The neuroprotective activity of our smart nanocarrier ANP:PNA:NGF was assessed *in vitro* on human retinal pigment epithelial cells and further investigated *in vivo* using the teleost zebrafish as animal model. Hence, we demonstrated that PNA not only improved the targeting of the posterior segment of the eye, thanks to its specific and high affinity for cone photoreceptors, but also prolongs the residence time of the NGF-based nanoformulation, thus resulting in a neuroprotective effect against retinal dysfunction induced by oxidative stress. Indeed, only the preventive administration of nanoformulated NGF, but not the free neurotrophin, improved the visual function of zebrafish larvae and provided a reduction of apoptotic cells in the retina in a model of oxidative damage induced through the intravitreal injection of hydrogen peroxide.

Finally, two novel models of retinal degeneration in zebrafish have been developed. Particularly, the effect of exogenous administration of cigarette smoke extract and all-*trans* retinal, an oxidized form of retinol, was studied to investigate their negative contribution on visual function in zebrafish larvae, also exploring the possible neuroprotective activity of ANP:PNA:NGF. Hence, data related to visual behaviour and differential expression of antioxidant genes were collected to provide insight into retinal degeneration caused by environmental factors, such as smoking and prolonged light exposure.

In conclusion, our multifunctional polymeric nanoformulation represents a promising strategy for implementing targeted treatment against retinal degeneration, also confirming the zebrafish as an extremely useful model organism for pre-clinical validations of nanomedicine-based drug delivery systems.

Abbreviations

AMD	age-related macular degeneration
ANPs	polyacrylamide nanoparticles
atRAL	all-*trans* retinal
Casp3a	caspase 3a
Cat	catalase
CSE	cigarette smoke extract
DLS	dynamic light scattering
DMSO	dimethyl sulfoxide
DPBS	Dulbecco's phosphate-buffered saline
dpf	days post-fertilization
DR	diabetic retinopathy
GCL	ganglion cell layer
Gpx1a	glutathione peroxidase 1a
H_2O_2	hydrogen peroxide
hpi	hours post-injections
INL	inner nuclear layer
IVT	intravitreal
NGF	nerve growth factor
Nrf2 and *nfe2l2a*	nuclear factor erythroid 2-related factor 2
OKR	optokinetic response
PFA	paraformaldehyde
PNA	peanut agglutinin
PRs	photoreceptors
RGCs	retinal ganglion cells
RNS	reactive nitrogen species
ROS	reactive oxygen species
RPE	retinal pigment epithelium
VEGF	vascular endothelial growth factor
VMR	visual motor response

1. INTRODUCTION

1.1 Structure of the human eye: focus on the retina

The eye is a globular sense organ that can be divided into the anterior and the posterior segments. The anterior segment, the front section of the eye, is constituted by 4 mainly interconnected structures, which are the cornea, the conjunctiva, the iris-ciliary bodies, and the crystalline lens, and it contains the aqueous humour. The posterior segment, the back section of the eye, contains the vitreous humour and consists of the sclera, the choroid, the retina, and optic nerve [1].

The functional sensory structure of the eye is constituted by the retina, which is responsible for converting light into electrical signalling to pre-process visual information, in a process called visual transduction [2]. The retina originates from the central nervous system and consists of retinal pigment epithelium and neural retina, which includes nervous and glial cell types finely organised in a multi-layered structure (**Figure 1**).

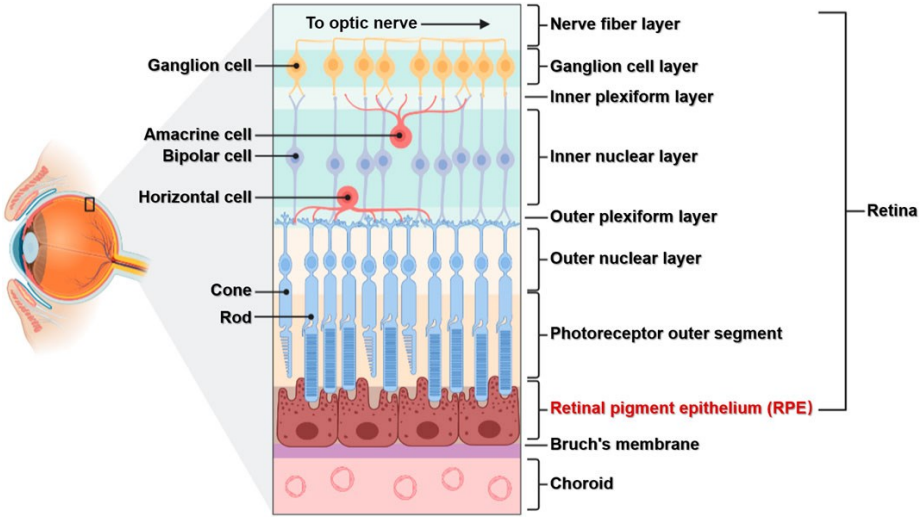

Figure 1. Structure of the retina. *Schematic representation of retinal nervous cell types and retinal layers. Image taken from Yang et al., Front Pharmacol. 2021.*

Particularly, it is possible to distinguish three nuclear layers, where the soma of cells is located, and two plexiform layers, where the synapses of retinal neurons are formed. The light-sensitive cells of the retina, such as cone and rod photoreceptors (PRs), are localised in the **outer nuclear layer** and their outer segments interact with the **retinal pigment epithelium**, a cellular monolayer which supports PRs metabolism. The **inner nuclear layer** consists of the soma of interneurons as bipolar, amacrine, and horizontal cells. The axons of bipolar cells form synapses with photoreceptors and with ganglion cells at the level of the **outer plexiform layer**

and the **inner plexiform layer**, respectively. The **inner plexiform layer** provides a connection between amacrine and horizontal neurons as well. The soma of ganglion neurons composes the **ganglion cell layer**, while their long axons are involved in the **optic nerve** formation, which sends synapses of ganglion cells to the visual cortex to complete the transmission of visual signals. Finally, both the **internal and external limiting membranes** are formed by the processes of Müller glia cells [3].

Several anatomical and physiological barriers provide protection to this sophisticated sense organ. Indeed, it is possible to distinguish between static and dynamic barriers (**Figure 2**).

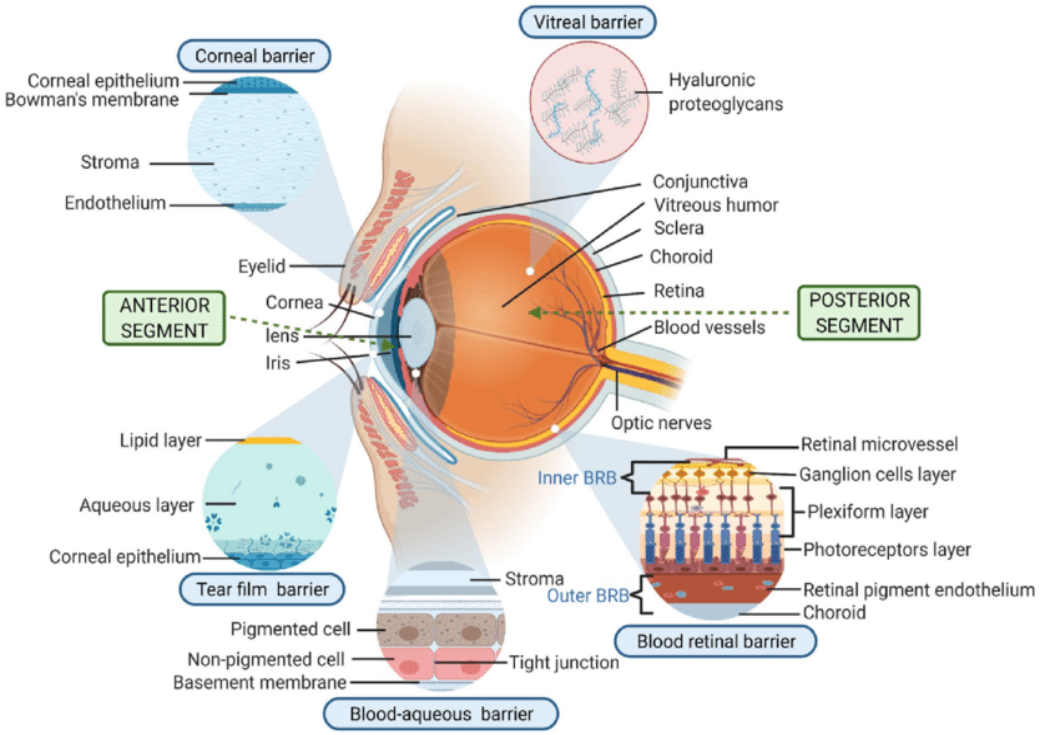

Figure 2. Ocular barriers. *Schematic representation of static and dynamic barriers included at both anterior and posterior segments of the eye. Image taken from Adriano et al., Drug Deliv Transl Res. 2022.*

The static barriers include anatomical boundary structures at both the anterior segment, such as the corneal epithelium and the blood-aqueous barrier (formed by the epithelium of ciliary body and the capillaries of the iris), and the posterior segment, such as the scleral, choroidal and the blood-retinal barriers. Particularly, the blood retinal barrier strictly limits the transport of molecules in the eye through the tight junctions between the endothelial cells of the retinal capillaries (inner part) and the retinal pigment epithelium (RPE) cells (outer part). Dynamic barriers comprise lacrimation and tear film (produced by the conjunctiva), intraocular flow processes, clearance mechanisms by aqueous and vitreous humour, and choroidal and conjunctival blood flow [4,5]. Ocular barriers are thus essential for protecting the organ and maintaining the ocular homeostasis; nevertheless, they limit the accessibility of therapeutics, making the treatment of ocular diseases challenging.

1.2 Retinal degenerative diseases

Ocular posterior segment diseases, including glaucoma, age-related macular degeneration, and diabetic retinopathy, represent a debilitating and increasingly frequent health problem worldwide. These pathological conditions are complex and multifactorial, but they share retinal degeneration as main clinical feature, which leads to partial or total vision loss. Globally, the World Health Organization estimated at least 2.2 billion people suffering from vision deficit or loss at the end of 2022 and more than 80% of them were aged 50 years or older. As vision is considered the most important sense for humans, its impairment negatively impacts independence and quality of life of the individuals affected by ocular posterior segment diseases. Moreover, the increase in ageing of global population results in a growing need for eye health services and a substantial financial burden [6].

Glaucoma includes a group of optic neuropathies characterized by elevated intraocular pressure, which results in the loss of ganglion cells and their axons (optic nerve), leading to peripheral or central irreversible blindness. It has been estimated that 76 million people worldwide have been affected by glaucoma in 2020, and this number is set to increase to 111 million by 2040 [7]. Although the increased intraocular pressure plays the major role in glaucoma pathogenesis, several risk factors have been identified, including older age, oxidative stress and inflammation, smoking, ethnicity, genetic background, vascular dysregulation, diabetes, and use of steroids [8,9]. No cure is available for glaucoma, but treatment options for lowering intraocular pressure include eye drops of therapeutic drugs to reduce the production of aqueous humour in the eye or increase its outflow, laser therapy or surgery [10].

Age-related macular degeneration (AMD) is the leading cause of irreversible blindness in patients over the age of 50 in developed countries. In 2020, the number of AMD patients worldwide was 196 million and is projected to increase to 288 million in 2040 [11]. The pathogenesis of AMD is multifactorial and includes dysfunction in inflammatory, angiogenic and oxidative stress-related pathways as well as exposure to ultraviolet radiation. Family history, smoking and ageing are the major risk factors associated with AMD [12]. Degeneration mainly occurs in the central retina (macula), leading to progressive central blindness. In fact, the disease is classified in two forms, known as dry AMD and wet AMD. Dry AMD represents the early-stage disease, and it is characterized by the presence of drusen (lipids and proteins deposit), degeneration of photoreceptors and changes in RPE cell pigmentation. Wet AMD is the late-stage exudative form of disease, where a pathological neovascularisation of the choroid occurs and causes geographic atrophy (chronic degeneration of the macula) and rapid vision loss [13]. No treatment is available for dry AMD, and preventive strategies for slowing its progression include having an antioxidant-rich diet, maintaining a normal weight,

exercising, and avoiding smoking. Treatment options for wet AMD includes IVT injection of anti-angiogenic drugs, including those targeting vascular endothelial growth factor (VEGF), photodynamic therapy, and laser photocoagulation to prevent or limit neovascularization [14].

Diabetic retinopathy (DR) is one of complications of diabetes and represents the major cause of blindness in the middle-aged and elderly people. DR is characterized by chronic hyperglycemia and is clinically classified into non-proliferative and proliferative forms in relation to the presence or absence of retinal neovascularization, with or without macular oedema [15]. In 2020, estimates reported 103.12 million of adult patients with DR worldwide, and the numbers are set to increase to 160.50 million by 2045 [16]. Hyperglycemia, hypertension, dyslipidemia, smoking, race, and higher body mass index are the main risk factors for disease development and progression. No cure is available for DR, but preventive actions, i.e., control of blood glucose, blood pressure and cholesterol level, as well as treatments, including injections of anti-VEGF drugs, panretinal laser photocoagulation and vitrectomy, can slow or arrest its progression [17].

1.3 Oxidative stress: key factor in retinal degeneration

The retina is a high metabolically active tissue, with abundant mitochondria performing oxidative phosphorylation and relying on aerobic glycolysis [18]. In the process known as visual cycle, light stimuli provoke phototransduction reactions of visual pigments in photoreceptors able to convert light into electric stimuli. Simultaneously, the conformationally-changed visual pigments are recovered for recycling in the RPE. In addition, the synaptic transmission of electric signals, from the photoreceptors to the brain through the optic nerve, demands a high intake of oxygen and nutrients from the blood cells. Consequently, these events require a considerable energy demand [19].

In the process of energy production, reactive oxygen species (ROS) and reactive nitrogen species (RNS) are generated. ROS include superoxide anion oxygen (O_2^-), hydrogen peroxide (H_2O_2), and the hydroxyl radical ($^{\cdot}OH$), while RNS derive from the reaction of nitric oxide with O_2^- [20].

ROS produced in physiological conditions are constantly removed by antioxidant systems, thus preserving homeostasis and eye health. Antioxidant systems, which also require ATP consumption for their repair functions, involve endogenous antioxidant enzymes, such as heme oxygenase 1, glutathione S-transferase, glutathione reductase, glutathione peroxidase, superoxide dismutase, and catalase [21]. Their expression is mainly upregulated by the transcription factor nuclear factor erythroid 2-related factor 2 (Nrf2), which is the master regulator of the cellular mechanisms in response to oxidative stress [22].

However, when the production of reactive species exceeds the limits of the detoxification system, thus an imbalance against their elimination occurs, they act as metabolites with a high capacity to oxidize proteins, lipids, and nucleic acids [23], thus culminating in autophagy and mitophagy processes [24,25], mitochondrial dysfunction [26], cell death and inflammation [27]. Indeed, high level of ROS activates NF-kB pro-inflammatory pathway [28] as well as caspase 3 pathway (mitochondrial-mediated apoptosis) [26] and caspase-independent apoptotic pathway [29]. This results in pathological changes of retinal microvasculature, neurodegeneration, and disruption of blood retinal barrier [30].

The high oxygen demand and metabolic rate of the retina, which contains abundant photosensitizers and fatty acids-rich cells exposed to visible light, offers a favourable environment for the oxidation. In fact, excessive or prolonged light stimulation of the retina, but also smoking and metabolic syndrome, such as diabetes and hypertension, causes a chronic condition of oxidative stress and retinal degeneration [31]. These pathological effects are furthering from the age-associated progressive decline of physiological functions and

constitute the shared and interconnected mechanisms at the basis of ocular degenerative diseases (**Figure 3**).

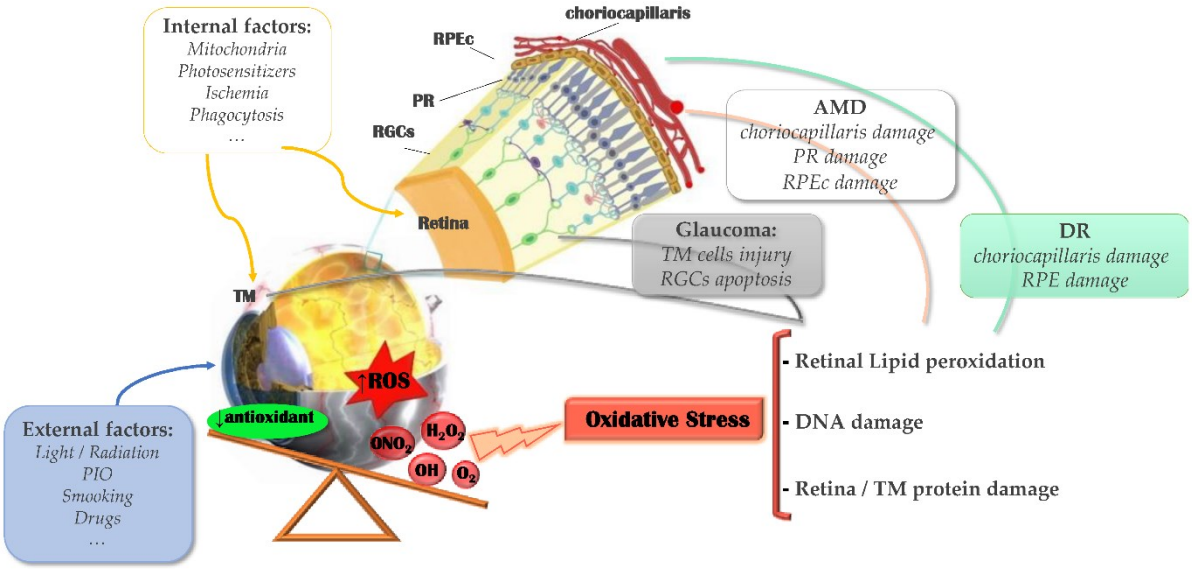

Figure 3. Schematic representation of the contribution of oxidative stress in the pathogenesis of ocular degenerative diseases. *Image taken from Dammak et al., Pharmaceutics 2021.*

As already described, the degeneration occurring in glaucoma is mainly caused by retinal ganglion cell (RGCs) death. RGCs are vulnerable to increased levels of oxidative stress due to their elevated oxygen consumption and high proportion of polyunsaturated fatty acid [32]. Mechanical pressure induced by elevation of intraocular pressure results in an inhibition of retrograde neurotrophin support to RGCs and in an alteration of mitochondria, which enhances the production of cytochrome c, ROS and RNS, and drives lipid peroxidation [33]. Moreover, according to the vascular theory, the RGCs death is also triggered by the generation of free radicals as consequence of an ischemic condition induced by an impaired blood flow in retinal vessels [34]. Additionally, RGCs apoptosis is responsible of ROS increase in a pathogenic feedback loop known as second-generation glaucoma [35].

In the early stages of AMD, a drastic reduction of phagocytic and metabolic activity of RPE cells occurs. The exposure to visible and ultraviolet light and high oxygen levels contribute to increase oxidation processes in the aging macula. Indeed, with light exposition, polyunsaturated fatty acids present in the photoreceptors cell membranes are easily oxidized and their accumulation further damage photoreceptors, RPE cells, and choriocapillaris [36]. Additionally, photoreceptor and RPE layers include postmitotic cells, which are not able to counteract the effects of defective mitochondria function during mitosis, thus leading to

accumulate mitochondrial mutations in aging RPE cells [37]. Lastly, oxidative stress leads to a condition of chronic inflammation in the AMD [28].

In DR, the disruption of the neuroglial-vascular units is firstly provoked by the hyperglycemia. Indeed, hyperglycemia-induced apoptosis causes the reduction of endothelial cells, which is followed by the increase of vascular permeability and capillary membrane thickening, thus resulting in edema and hemorrhages [38]. In addition, the generation of ROS in the mitochondria compromises the function of the electron transport chain, thus increasing the amount of superoxide even with normal levels of glucose [39]. Furthermore, ROS stimulates inflammation and angiogenesis by activation of the pro-inflammatory NF-kB and hypoxia-inducible factor-1 (HIF-1) pathways [28,40], thus contributing to the pathogenesis of both diabetic micro and macrovascular complications.

1.4 Administration routes for targeting the ocular posterior segment

The complex anatomical structure and the physiological mechanisms that protect the eye make the delivery of drugs a challenging goal. Different routes are available for targeting the ocular posterior segment (**Figure 4**).

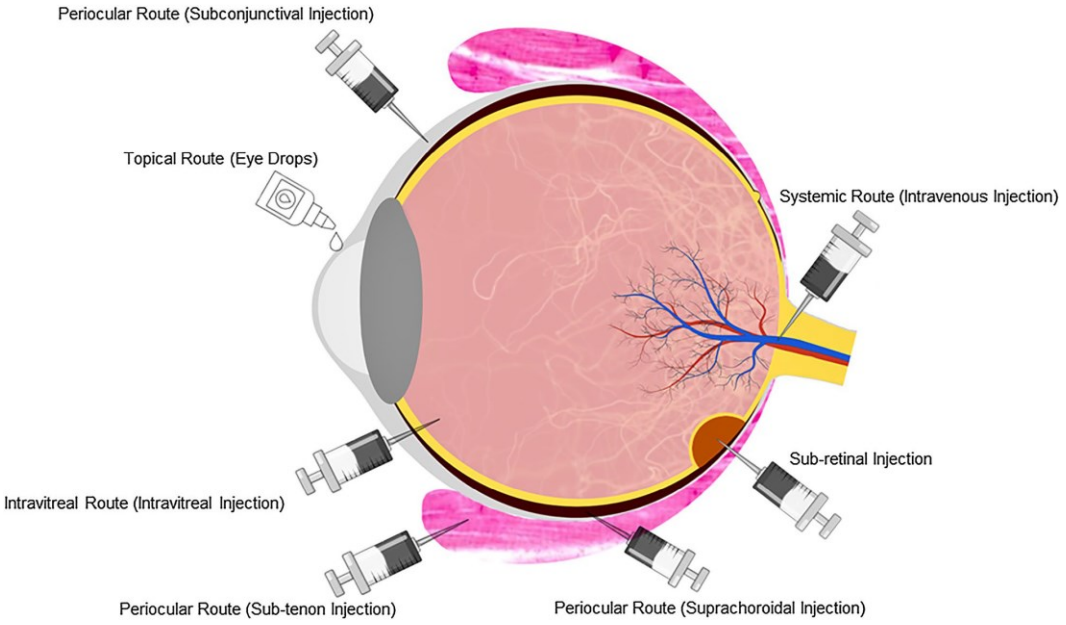

Figure 4. Routes of administration for ocular drug delivery. *Topical, systemic, and local routes are represented. Image taken from Karamali et al., J Transl Med. 2022.*

Topical and systemic delivery represents non-invasive and patient-friendly routes for administering therapeutics to the eye. However, the multiple barriers present from the ocular surface to the back of the eye limit the penetration of therapeutics. In fact, less than 5% of drugs instilled with eye drops reaches the ocular posterior segment, while the retinal penetration of drugs by intravenous injection is hampered by the presence of blood retinal barrier and its efflux transporters [41,42]. The periocular route, which includes sub-tenon, subconjunctival and suprachoroidal injections, is the delivery of therapeutics into the periocular tissue. However, even if the administration is local, thus minimizing systemic toxicity, it still requires a high volume of drug and displays several disadvantages, including pain, haemorrhages, orbital swelling, optic nerve damage and retinal ischemia. The sub-retinal route allows the direct injection close to the retinal cells and it is considered the most efficient route for administering cell and gene therapies. However, it can be performed only in one step to avoid retinal detachment and requires professional surgical skills. The gold standard for the ocular posterior segment treatment is represented by the intravitreal route, which consists in

the direct administration of drugs into the vitreous. The local delivery allows to overcome many ocular barriers; nevertheless, it needs several injections to guarantee drug release over time in an optimal therapeutic dose. Sadly, this requirement may lead to infection, ocular pain, and haemorrhage, thus resulting in patient discomfort and poor compliance [5].

As a result, the clinical success of a therapy able to counteract retinal degeneration strongly depends on the selection and optimisation of the best method of drug delivery to the ocular posterior segment. Research aims to develop strategies for improving drug permeation through ocular barriers, prolonging drug residence time, and providing a controlled and targeted release.

1.5 Therapeutic strategies against vision loss

Therapeutical approaches against retinal degeneration can be divided into four different categories: cell therapy, visual prosthesis, gene therapy and neuroprotection strategies [5] (**Figure 5**).

Figure 5. Therapeutical interventions against retinal degeneration. *Image modified from Karamali et al., J Transl Med. 2022.*

Cell-based therapy refers to the replacement of injured retinal cells with incompletely differentiated cells by ocular injection of cell suspension or tissue transplantation at the sub-retinal space. The injection of fetal human retinal progenitor cells in 8 patients with retinitis pigmentosa resulted in a significantly improved visual acuity and an increased retinal sensitivity of pupillary responses in a phase I clinical trial [43]. However, ethical and regulatory limitations demand the use of pluripotent stem cells, such as human embryonic stem cells (hESCs) and induced pluripotent stem cells (iPSCs) as alternative [44]. Several trials investigated cell therapy approaches based on hESCs- or iPSCs-derived RPE cells as treatment for age-related macular degeneration and Stargardt's macular dystrophy. Phase I and II studies showed good safety profiles, but the long-term safety and efficacy still need to be proved [45].

Visual prosthesis refers to electronic devices composed by an external video camera, which captures images from the outside, connected to an implanted microelectrode array, which convert the transmitted data into electrical stimulation. Different prosthetic devices are

commercially available, including Argus II epiretinal device and Alpha IMS (NCT00407602, NCT01024803). A promising alternative for avoiding drawbacks associated with the implantation of array components is represented by a nanoparticles-based liquid retinal prosthesis recently developed. In this study, semiconducting polymer-conjugated nanoparticles sub-retinally injected in a rat model of retinitis pigmentosa were able to widely diffuse through the subretinal space and generate light-evoked stimulation of inner retinal neurons [46]. However, prosthetics only allow an artificial vision and significant challenges are still pending for restoring vision.

Gene therapy represents a powerful strategy for the treatment of inherited retinal diseases (IRD) by delivering genetic material through viral and non-viral vectors. Particularly, the development of naked DNA, liposomes and nanoparticles as gene carriers is underway to reduce immunogenicity, pathogenicity and costs in comparison to approaches based on viral carriers [47]. Indeed, although the viral vector-based formulation Luxturna™ is the only FDA-approved gene therapy for treating a subset of patients (RPE65 mutation) with IRD [48], no evidence to determine long-term safety and efficacy of the treatment are available. Importantly, the therapy is not approachable for the large majority of IRD patients for both individual genetic background and costs issues. Only certain populations of the small subset of patients with the RPE65 mutation could benefit from the treatment, and the cost of $850,000 is unaffordable to many of them. Moreover, despite the adeno-associated virus 2 (AAV2) is the preferred viral carrier to deliver genetic material into the retina, thanks to its mild immunogenicity, not pathogenicity and stable gene expression, its gene packaging capacity is limited (<5 kb). Consequently, other approaches must be developed to implement therapies for inherited retinal diseases, such as Stargardt's disease and Usher syndrome type IB, which require the delivery of larger genes. Lastly, although the safety of the treatment Luxturna™ has been confirmed to date, common adverse reactions, such as retinal deposits, ocular inflammation, cataract and increased intraocular pressure have been registered [49]. As an alternative, several studies reported promising pre-clinical results achieved using nanoparticles-based gene delivery and CRISPR/Cas9-mediated genome editing in the retina [50,51]. Additionally, recent data from the Phase 1/2 BRILLIANCE trial, an *in vivo* CRISPR/Cas9 gene editing to correct CEP290 mutation causing Leber Congenital Amaurosis, provided results of safety delivery and consistent efficacy in 3 out of 14 treated subjects (NCT03872479). Unfortunately, although the clinically meaningful improvements, the development of the therapy and the enrollment of patients have been paused due to the small population of responders (patients carrying a homozygous mutation), thus saving commercial interests at the detriment of patients' health [52]. Future developments are thus needed to

provide a long-term expression through non-viral gene delivery methods and overcome the off-target effect associated with the CRISPR/Cas9 technology.

Neuroprotective strategies aim to slow and prevent the progression of visual impairment. Most pre-clinical and clinical studies related to the development of neuroprotective treatments are based on the use of antioxidants and neurotrophic factors [53]. Indeed, both internal and external pathological factors involved in retinal degeneration trigger oxidative stress, which is strictly associated with other molecular pathways implicated in disease progression. However, analysis of clinical data showed a limited or absent efficacy of diets supplemented with antioxidants or natural extracts in improving visual function or reducing the progression of glaucoma, AMD and DR [27]. Conversely, use of neurotrophins in retinal degeneration for promoting cell survival and maintenance showed promising effects in several investigations. In a mouse model of retinal degeneration, the stimulation of Müller cells with glial-derived neurotrophic factor (GDNF) induced the release of neurotrophic factors, which promoted photoreceptor survival [54]. Similarly, the sub-retinal injection of GDNF-loaded nanoparticles in a mouse model of light-induced retinal degeneration resulted in histological and functional rescue of photoreceptors [55]. The delivery of ciliary neurotrophic factor (CNTF) by encapsulation into intraocular implants was well-tolerated and resulted in a dose-dependent increase in retinal thickness and reduction of vision loss progression in clinical studies for the treatment of retinitis pigmentosa and geographic atrophy, respectively [56,57]. The beneficial effect of brain-derived neurotrophic factor (BDNF) in reducing RGCs and vision loss and preserving visual function has been showed in mouse models of glaucoma [58,59]. Finally, a huge body of evidence demonstrated pro-survival and regenerative effects of NGF in pre-clinical and clinical models of glaucoma [60-62], DR [63], AMD [64], and retinitis pigmentosa [65,66]. Nevertheless, neurotrophin-based therapies are at the very early stages of market approval and clinical applicability due to several drawbacks that still require a solution, such as their poor solubility, low delivery efficiency, short half-life, and off-target effect [67]. Such drawbacks can be overcome by the application in ophthalmology of nanotechnological-based strategy, as discussed in the following section.

1.6 Nanomedicine in ophthalmology

Nanotechnology refers to the use of materials with at least one dimension at the nanometric scale and its application in the diagnosis and treatment of diseases is known as nanomedicine [68].

The application of nanotechnology in the ophthalmic field has been introduced since 1980s, with the aim to improve the properties of conventional drugs in terms of overcoming ocular barriers (i.e., enhancing corneal permeability) and improving solubility and stability, thereby reducing degradation, and prolonging the bioavailability and ocular retention of drugs. In the last 20 years, the number of nanotechnology-based formulations used for ocular drug delivery is indeed increased. As a matter of fact, nanomaterials represent a minimally invasive method in ophthalmology, thanks to the physicochemical properties of materials at the nanoscale, offering a wide range of characteristics to improve pharmacokinetic and pharmacodynamic drug profiles [69]. In relation to their chemical composition, nanomaterials can be distinguished in organic, including liposome, micelle, dendrimer, and polymers, and inorganic nanocarriers, composed of carbon, silica, gold, silver, or iron oxide [70].

Nanoparticles possess a high surface-to-volume ratio, which allow to embed a variety of molecules, including drugs, peptides, proteins, or nucleic acids, thus increasing their solubility, stability, and bioavailability by protecting them from degradation [71]. Due to their nanoscale size and surface characteristics, nanocarriers display better interactions with conjunctival and corneal epithelium, can permeate the capillaries via the blood flows and pass across the ocular barriers [72]. Moreover, thanks to the presence of functional groups on their surface, which can serve as binding site for several molecules through absorption or covalent binding, nanocarriers can be externally functionalised, thus providing a targeted drug delivery in specific cells or tissues [73]. The precise drug delivery as well as the extended retention of molecules for a sustained release over time represent the most appealing characteristics for implementing a nanosystem for the posterior segment of the eye. Indeed, the exploitation of nanocarriers, which allow targeting and enhance sustainability, residence time and intraocular bioavailability, results in increased therapeutic efficiency, permitting to reduce drug dosage and restraining the administration frequency [74]. Consequently, the pharmacological improvement of drug profiles translates into the reduction of side effects and the amelioration of patient compliance and quality of life.

1.6.1 Clinical trials and FDA-approved nanomedicines

The application of nanomedicine in ophthalmology mainly aims to develop strategies against retinal degeneration and involves the use of drug delivery systems, implantable materials, implantable devices, and diagnostic tools [75]. Although numerous FDA-approved nanoformulations are commercially available, they are mainly addressed to the treatment of diseases affecting the anterior segment of the eye, including dry eye disease, eye inflammation and infections [69].

Nanostructured drugs targeting the ocular posterior segment only includes Visudyne®, a liposome-based nanoformulation of verteporfin, and Macugen®, a pegylated anti-VEGF aptamer, which are applied in the treatment of choroidal neovascularization related to AMD and wet AMD, respectively. FDA-approved innovative slow release systems are commercially available also for the treatment of macular edema, including intravitreal implants, such as Ozurdex® (dexamethasone) and Iluvien® (fluocinolone acetonide), and microparticles suspensions administered by IVT injections, such as Triesence® (triamcinolone acetonide) and Kenalog® (triamcinolone acetonide). In addition, several clinical trials are ongoing for meeting the urgent clinical need to find therapies against retinal degeneration. Latanoprost coated liposome (POLAT-001) and latanoprost-punctum plug delivery system completed phase II clinical trial for the treatment of glaucoma (NCT02466399, NCT00650702), while IVT implants of dexamethasone sodium phosphate (Ozurdex®) or brimonidine tartrate are currently in phase III and II clinical trials as promising treatments for AMD (NCT00168389, NCT00658619). Despite the considerable advances of nanomedicine in the field of ophthalmology in the last 20 years, its success in terms of clinical translation is still impaired by the lack of late-phase clinical trials and the limited industrial development and scalability of nanoformulations [76].

1.6.2 Pre-clinical studies

Despite no cure is available to restore vision, both organic and inorganic nanoformulations are deeply investigated as promising drug delivery systems for counteracting vision loss and delay disease progression [77].

Polymeric nanoparticles represent the key element in different drug delivery strategies. They are developed from synthetic and natural biocompatible and biodegradable polymers and can be exploited in both ocular drug and gene delivery [4]. Among them, polymeric acrylic nanoparticles possess exclusive properties that make them suitable for drug delivery applications. The high stability and biocompatibility of poly-acrylic derivatives have been widely studied and the presence of numerous functional groups perfectly addresses the need

to load drugs and enable their sustained release, further enhanced by their unique properties of being responsive to external and internal stimuli [78]. Although commercially available nano-based systems for the treatment of ocular diseases are limited, both pre-clinical and clinical studies show promising results in the development of nanoformulated drugs against retinal degeneration. Dind and co-authors demonstrated that annexin V-conjugated cubosomes entrapping LM22A-4, a neurotrophic factor mimetic, were able to target the posterior segment, prevent RGCs loss and improve functional outcomes in a mouse model of glaucoma [79]. Qui and co-authors reported a controlled drug release profile for more than 60 days of fenofibrate (a peroxisome proliferator-activated receptor α agonist) after its loading into biodegradable poly(lactic-co-glycolic acid) nanoparticles. Results showed no toxicity of retinal structure and function in rat models of DR and neovascular AMD. Particularly, one single IVT injection of PLGA-loaded fenofibrate resulted in a reduced retinal vascular leakage in both models and an amelioration of retinal dysfunction in diabetic rats [80].

Despite the huge body of studies supporting the potential benefits of applying nanomedicine in the ophthalmological field, several drawbacks, which hampers clinical implementation of nano-based technologies, still need to be addressed. Indeed, several studies are yet restricted to *in vitro* assessments or mainly use rodent models for testing the efficacy of nanoformulations. However, although the size of the rabbit eye is comparable to humans, this rodent model displays several differences with respect to humans, including an increased mucus production and surface sensitivity and a reduced tear production and blinking frequency, resulting in different profiles of ocular bioadhesion and retention, which do not completely resemble human physiology [81]. Consequently, several evidence are still required to fill gaps related to toxicity, efficacy, dispersion safety, preparation reproducibility, and industrial scale up of nanomaterials, in order to empower pre-clinical findings and progress toward clinical development.

1.7 Zebrafish as a pre-clinical model for studying retinal degeneration

The teleost zebrafish (*Danio rerio*) are freshwater fish originating from India who became an appealing and widely established model organism in biomedical research [82]. Indeed, many advantages are associated with their use in pre-clinical studies, including small size, ease of handling, *ex utero* fertilization, high fecundity (100-200 embryos per breeding pair), rapid development, transparency of embryos and low costs [83]. Zebrafish gained popularity to study retinal degeneration and visual dysfunction due to the high genome homology (70% of human genes have at least one zebrafish orthologue, with 84% of known human disease-causing genes having a zebrafish counterpart) and the same anatomical and cell-layered retinal structures shared with humans [84,85]. Indeed, it is possible to distinguish the ganglion cell, inner cell, and photoreceptors layers as well as the same stratification of neuronal and glial cell types as humans (**Figure 6**).

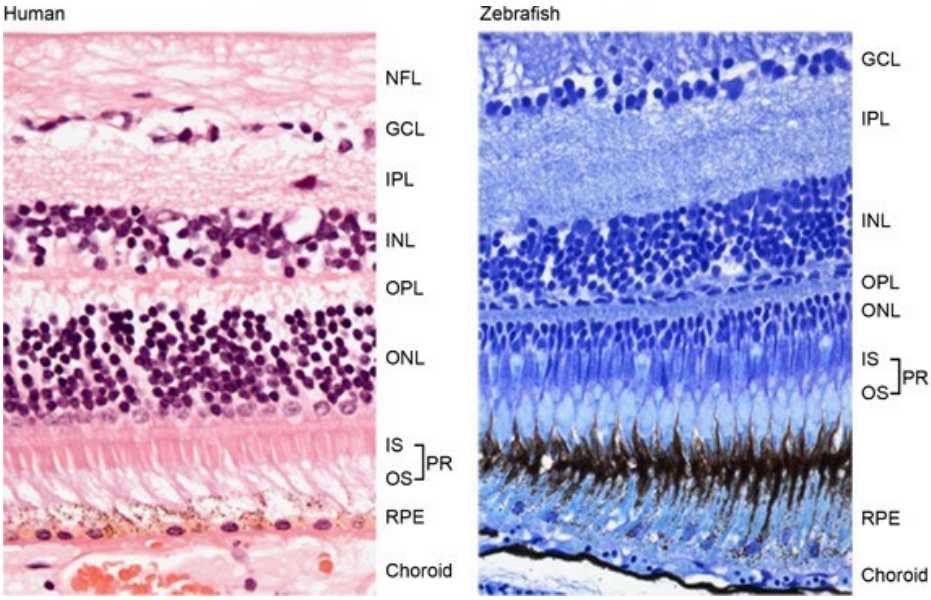

Figure 6. Histological cross-sections of human and zebrafish retina. *Retinal stratification and cell types are shared across humans and zebrafish. Image taken from Richardson et al., Eye (Lond). 2017.*

Conversely to rodent models, zebrafish share with humans a cone-mediated vision, but possess UV-cones in addition [86]. Due to their extremely rapid development, visual function is well-established already at 3 days post-fertilization (dpf) and several visual behavioural assays can be performed, thus allowing to run consistent short-term studies at early stages of development [87]. Thus, zebrafish are increasingly being employed to conduct nanotoxicological studies and pre-clinical validation of modern drug delivery formulations [88,89]. Taking advantage of their great homology with the human eye as well as the ease of

manipulation, zebrafish larvae were already used by our group as pre-clinical model to test both safety and efficacy of a new nanoformulation. Indeed, as reported in the literature, we previously implemented a model of oxidative stress in the eye of zebrafish larvae by performing IVT injections of hydrogen peroxide, which was successfully used to assess the neuroprotective activity of a novel nanotool obtained by the combination of neurotrophins with magnetic nanoparticles [90]. Importantly, the possibility of performing time-saving and high-throughput experiments in a living organism is given by the low ethical impact. Indeed, zebrafish are considered non-sentient organisms until 5 dpf in accordance with the EU directive 2010/63/EU for protection of animals used for scientific purposes.

2. AIM OF THE STUDY

The aim of the Ph.D. project is to implement a nanomedicine-based strategy against retinal degeneration through the development of smart nanoparticles able to target the ocular posterior segment and enhance the bioavailability of drugs. Indeed, these nanocarriers-based approach might offer a potential strategy to overcome the failure of therapies related to poor drug delivery and unfavourable kinetics and drug retention at this site. Indeed, the complex anatomical structure and the ocular physiology hinder the delivery of drugs in the posterior segment, thus resulting in the lack of effective treatments able to counteract retinal degeneration and visual impairment.

The research focused on two main aspects, including the development of different types of nanoparticles for pursuing neuroprotection in retina, and the implementation of pharmacological modulation of visual function *in vivo* using zebrafish larvae as model system. Organic polyacrylamide-based nanoparticles have been selected and optimised for obtaining a polymeric multi-functional nanocarrier for ocular drug delivery through the functionalisation with peanut agglutinin (PNA) as targeting molecule and nerve growth factor (NGF) as a neuroprotectant. The neuroprotective efficacy of the nanosystem against visual dysfunction induced by oxidative stress has been validated *in vivo* using zebrafish at larval stage, and promising results have been collected by both behavioural and functional assessments.

In parallel, all-*trans* retinal (atRAL) and cigarette smoke extract (CSE) were investigated as potential novel pharmacological models of retinal degeneration with the aim to deepen knowledge about their contribution to visual impairment in humans and evaluate preventive therapeutical strategies, including the neuroprotective nano-based formulation here developed.

3. MATERIALS AND METHODS

3.1 Polyacrylamide nanoparticles (ANPs)

3.1.1 Synthesis

Polyacrylamide nanoparticles composed by *N*-Isopropylacrylamide (NIPAM), acrylamide (AAm), allylamine hydrochloride (AH) and *N*,*N*′-Methylenebisacrylamide (BIS) were synthesised by optimising the radical polymerization protocol developed by Rahimi and colleagues [91]. 222 mg of NIPAM (#731129, Merck), 28.6 mg of AAm (#A9099, Merck), 76 mg of AH (#735132, Merck) and 262 µL of 2% BIS solution (#M1533, Merck) were dissolved in 10 mL of de-ionized water previously purged with argon at room temperature and under stirring. 11.5 µL of 10% sodium dodecyl sulfate (SDS; #436143, Merck) solution was added and the solution was purged with or without argon for 30 min. To obtain fluorescent nanoparticles, 1 mg of Alexa Fluor 488 (#A20000, Invitrogen) or Alexa Fluor 594 (#A20004, Invitrogen) dyes were dissolved before to stop the argon flow and 15.6 mg of ammonium persulfate (APS; #A3678, Merck) and 20 µL of N,N,N′,N′-Tetramethyl ethylenediamine (TEMED; #T9281, Merck) were added. Finally, de-ionized water was added to the final volume of 20 mL and the reaction was carried out at room temperature for 3, 4, 8 or 24 h under continuous stirring in darkness. Different reactions were set up, modifying some parameters as previously indicated (**Table 1**). Dialysis was performed by transferring the sample into a 10 kDa cut-off membrane kept in de-ionized water under stirring and replacing with new water each hour per 4 times. Finally, the sample was concentrated in a 30 kDa Vivaspin® tube (Sartorius) by centrifuging at 3000 x g until obtaining 1 mL of nanoparticles suspension and kept at 4 °C.

Fluorescent dye	Argon flux	Reaction time
Alexa Fluor 488	Yes	3 h
Alexa Fluor 594	Yes	3 h
-	No	4 h
-	No	8 h
-	No	24 h

Table 1. Radical polymerisation reactions using different parameters for the synthesis of polyacrylamide nanoparticles.

3.1.2 Characterization of the hydrodynamic diameter

The size distribution and the polydispersity index of naked, single- and double-functionalised ANPs were assessed by dynamic light scattering (DLS) using a Zetasizer NS (Malvern Instrument). Each sample was diluted 1:1000 in water before any measurements and the index of refraction was set at 1.45.

3.1.3 Functionalisation with peanut agglutinin (PNA)

ANPs coated with FITC-conjugated PNA from *Arachis hypogaea* (#L7381, Merck) (ANP:PNA) were obtained through a non-covalent functionalisation of the particles by incubating 1:1 ratio of ANPs and PNA at 4 °C for 1.5 h under stirring. The sample was concentrated using a 100 kDa Vivaspin® tube (Sartorius), washed with de-ionized water and kept at -20 °C in a 20% glycerol solution, while the eluate derived from the washing steps was stored for further analysis.

3.1.4 Functionalisation with nerve growth factor (NGF)

The functionalisations with native mouse NGF 2.5 S protein (#N-100, Alomone labs), alone or in addition to PNA, were carried out by incubating 1:1 ratio of ANPs and NGF (ANP:NGF) or 1:1:1 ratio of ANPs, PNA and NGF (ANP:PNA:NGF), respectively. The reactions were set up following the same protocol as above.

3.1.5 Peanut agglutinin binding efficiency through BCA assay

The concentration of PNA conjugated to the ANPs was estimated by BCA assay (Pierce™ BCA Protein Assay Kit; #23227, Thermo Scientific), according to the manufacturer's protocol. The concentration of PNA attached to the ANPs' surface was extrapolated by subtracting the mass of protein detected in the eluate to the total mass of protein used for carrying out the functionalisation. The protein content in the eluate was evaluated by measuring the absorbance at 562 nm.

3.1.6 NGF binding efficiency through ELISA assay

An ELISA assay (Mouse beta-NGF ELISA Kit; #RAB1119, Merck) was performed to evaluate the amount of NGF bound to ANPs and ANP:PNA. Both quantifications were performed by using the eluate derived from the washing steps of the functionalisation reactions. The concentration of NGF attached to ANPs and ANP:PNA surface was extrapolated through subtraction, as previously described, by measuring the eluate absorbance at 450 nm.

3.2 Bioactivity assessment of nanoformulated NGF

3.2.1 PC12 cell line cultures

Rat pheochromocytoma PC12 cells were obtained from the American Type Culture Collection (ATCC) and cultured in T25 flasks coated with 10 µg/mL poly-L-lysine using Dulbecco's Modified Eagle's Medium (DMEM; #21969, Gibco) supplemented with 10% horse serum (HS; #16050, Gibco), 5% fetal bovine serum (FBS; #10270, Gibco), 1% penicillin/streptomycin (Pen Strep; #15140, Gibco) and 2 mM L-glutamine (GlutaMAX™; #35050, Gibco) in humified atmosphere with 5% CO_2 at 37 °C. For the differentiation, PC12 cells were seeded at low density (2.5×10^4 cells per cm^2) and maintained in DMEM with 1% FBS and 100 ng/mL NGF for 4 days. Then, cells were washed with DPBS and fixed with 2% paraformaldehyde (PFA; #P6148, Merck) at room temperature for 10 minutes.

3.2.2 Neurites length analysis

Images were acquired at 10X magnification using a Nikon Eclipse TE2000-U microscope and the length of 180 neurites (randomly selected) was quantified by using the plugin *NeuronJ* available on *ImageJ* software. Neurites in networks were excluded. Independent experiments were performed, n=3.

3.3 *In vitro* model of oxidative stress

3.3.1 ARPE-19 cell line cultures

Human retinal pigment epithelial ARPE-19 cells were obtained from the American Type Culture Collection (ATCC). Cells were maintained in DMEM F-12 Ham (#D6421, Merck) supplemented with 10% FBS (#10270, Gibco), 2% penicillin/streptomycin (Pen Strep; #15140, Gibco) and 2 mM L-Glutamine (#25030, Gibco) in a humidified atmosphere with 5% CO_2 at 37 °C.

3.3.2 Cell treatments

Cells were seeded at density of 10×10^3 cells per well in a 96-well plate. After 24 h, cells were incubated with increasing concentration of hydrogen peroxide (200, 250, 300, 350, 400 or 600 µM H_2O_2; #H1009, Merck) to establish the minimum concentration needed to reduce cellular metabolic activity. Untreated cells were used as negative control.

For evaluating the neuroprotective activity of nanoformulated NGF, cells were co-incubated with 100 ng/mL of free or ANP:PNA-conjugated NGF and 300 µM hydrogen peroxide (H_2O_2; #H1009, Merck). Untreated cells were used as negative control, while positive control group was only treated with 300 µM H_2O_2. After 24 h, the treatment solutions were removed, and the MTT assay was performed.

3.3.3 MTT assay

To assess cellular metabolic activity, 100 µL of 0.5 mg/mL thiazolyl blue tetrazolium bromide (#M5655, Merck) solution were added and cells were incubated for 2.5 h. Then, 100 µL of DMSO (#276855, Merck) were added and incubated for a few minutes on a plate shaker to dissolve the water-insoluble formazan salts. Quantification was carried out using a CLARIOstar microplate reader and the absorbance was measured at 595 nm. 3 technical replicates were performed for each independent experiments, n=3.

3.4 Zebrafish model

3.4.1 Ethics statement

Animals were handled in compliance with protocols approved by the Italian Ministry of Public Health, the local Ethical Committee of the University of Pisa and by the University College Dublin (UCD) Animal Research Ethics Committee, in accordance with EU legislation (Directive 2010/63/EU). The manipulations conducted in this thesis are not classified as procedures, since the zebrafish model used was at the larval stage within 5 days post-fertilization (dpf).

3.4.2 Zebrafish husbandry

Zebrafish were maintained in an automated recirculating water system under a 14-hour light 10-hour dark cycle. The water system was set at the following parameters, according to guidelines provided by the Zebrafish Information Network [92]: temperature 28 °C, pH 7 and conductivity 700 µS. Adult zebrafish were fed with dry pellets and brine shrimp (*Artemia salina*) twice per day. Zebrafish embryos were obtained by natural spawning of wild-type fish and raised in Petri dishes containing E3 embryo medium (5 mM NaCl, 0.17 mM KCl, 0.33 mM $CaCl_2$, 0.33 mM $MgSO_4$) at 28 °C.

In accordance with the scientific animal protection legislation in Ireland, governed by the Health Product Regulatory Authority (HPRA), zebrafish larvae under 131 hours post-fertilization (hpf) raised at 27 °C are not considered protected animals. Therefore, for the experiment carried out at UCD, larvae were maintained in E3 embryo medium (0.137 M NaCl, 5.4 mM KCl, 5.5 mM Na_2HPO_4, 0.44 mM KH_2PO_4, 1.3 mM $CaCl_2$, 1.0 mM $MgSO_4$ and 4.2 mM $NaHCO_3$) containing methylene blue at 27 °C and humanely killed before 131 hpf by placement at -20 °C.

Before any intravitreal (IVT) microinjection, larvae at 3-, 4- or 5-dpf were anesthetized with 0.16 mg/mL tricaine (MS-222; #A5040, Merck) and embedded in 0.3% agarose (#A9539, Merck).

3.4.3 Model of retinal degeneration induced by oxidative stress

To study the neuroprotective activity of NGF-based polymeric nanoformulations, an oxidative condition was induced in the retina of larval zebrafish by following the protocol previously described by Giannaccini and co-authors [90]. Briefly, 5 dpf larvae were IVT microinjected into the left eye with 2 nL of 1 M H_2O_2 (#H1009, Merck) after 16 h from the preventive injection of free or nanoformulated NGF. 2 nL of DPBS were IVT injected as negative control.

3.4.4 Drug treatment

4 dpf larvae were placed in 6 cm Petri dishes and immersed in E3 embryo medium containing 20 or 25 µg/mL cigarette smoke extract (CSE) or 15 µM *all-trans* retinal (atRAL) for 4, 8 or 24 h. Larvae treated with 0.05% DMSO (#D2650, Merck) solution were used as negative control. Before any further experiments, drug-treated larvae were washed 3 times with fresh embryo medium.

To study the neuroprotective activity of free or nanoformulated NGF, 1 ng of NGF or ANP:PNA:NGF was IVT microinjected in larvae at 4 dpf. After 16 hours post-injection (hpi), larvae were exposed to 20 µg/mL CSE or 15 µM atRAL for 24 h.

3.5 Localisation studies of polymeric nanoparticles in zebrafish retina

3.5.1 OCT embedding and cryosectioning

2 nL of Alexa Fluor 488-positive ANPs were IVT microinjected in the left eye of 3 dpf larvae. Larvae were firstly observed with a Nikon SMZ18 stereomicroscope using both bright field and FITC channels to check the fluorescence *in vivo*. Then, they were fixed after 4, 8 and 24 hpi with 4% PFA at room temperature for 10 minutes, embedded in OCT and sliced with a cryostat to obtain 10 μm cross-sections. Sections were stained with Hoechst 33342 (#H3570, 1:1000, Invitrogen) and imaged at 20X magnification in bright field, DAPI and FITC channels using a Nikon Eclipse T*i* microscope. The presence of green signals at the at the different retinal layers was qualitatively evaluated, and data were plotted using *GraphPad Prism*. Each experiment was performed on 15 larvae per group.

3.5.2 Fluorescence microscopy

2 nL of naked (Alexa Fluor 594-positive) ANPs or ANP:PNA or DPBS were IVT microinjected in the left eye of 3 dpf larvae. The injected eyes were *in vivo* imaged at 4 and 24 hpi with a Nikon SMZ18 stereomicroscope, using bright field, TRITC and FITC channels to check the fluorescence of Alexa Fluor 594 and the PNA:FITC, respectively.

3.6 Behavioural assays

3.6.1 Optokinetic response (OKR) assay

The optokinetic response (OKR) was assessed in zebrafish larvae at 5 dpf after 8 hpi of H_2O_2. Larvae were embedded in 6% methylcellulose in a 3.5 mm Petri dish and placed in the center of a drum [93]. The ocular movements (saccades) of the left eye were measured for one minute in response to the rotation of a drum with black and white illuminated stripes moving at ~11 rpm. Each experiment was performed on at least 9 larvae per group, n=4.

Standard OKR using a 0.02 cycles per degree (cpd) drum was carried out after 24 h from the exposure to CSE or atRAL, according to the protocol previously published by Gómez Sánchez [94]. Each experiment was performed on at least 8 larvae per group, n=3.

3.6.2 Visual motor response (VMR) assay

Visual motor response (VMR) was performed as previously described in the literature [95]. Each larva was placed in a 96-well plate and immersed in 600 µL of embryo medium. 12 larvae were used per treatment group. The plate was placed in the Zebrabox recording chamber (Viewpoint Life Sciences, France) to record larval locomotor activity in response to acute changes in light intensity for a period of 1 h and 40 min. After 30 min of adaptation to the new environment, the light intensity changed from ON to OFF and vice versa in intervals of 20 min. Locomotor activity data were exported to *MS Excel* and analysed using *GraphPad Prism*. The activity of individual larvae was measured in milliseconds per second (ms/s) and three main parameters were analysed for each treatment group:

1. the average overall activity over 1 h and 40 min
2. the maximum activity recorded during the first 5 sec following the ON-OFF light change, defined as MAX OFF peak activity
3. the maximum activity recorded during the first 5 sec following the OFF-ON light change, named MAX ON peak activity

Each experiment was performed on at least 10 larvae per group, n=3

3.7 Functional study: evaluation of oxidative stress-triggered apoptosis

3.7.1 TUNEL assay

8 h after the induction of oxidative stress, larvae were fixed with 4% PFA at 4 °C overnight, embedded in OCT and sectioned (8 µm). Slices were washed with 1X PBS to remove OKR residuals and fixed with 4% PFA at room temperature for additional 20 min. Then, sections were stained using *In Situ* Cell Death Detection Kit, Fluorescein (#11684795910, Roche), according to the manufacturer's instructions, and Hoechst 33342 (#H3570, 1:1000, Invitrogen). Sections were imaged at 20X magnification in DAPI and FITC channels using a Nikon Eclipse T*i* microscope and the number of TUNEL-positive cells at the different retinal layers was quantified and plotted on *GraphPad Prism*. A single experiment was performed on at least 4 larvae per group.

3.7.2 Immunostaining of zebrafish retina

8 h after the induction of oxidative stress, larvae were fixed with 4% PFA at 4 °C overnight and maintained in bleach solution (0.18 M KOH and 3% H_2O_2 in ddH_2O) for 40 min at room temperature for removing the pigmentation of the RPE. The whole-mount immunostaining was carried out following an optimised protocol for zebrafish retinal samples [96]. To enhance tissue permeabilization, larvae were first heated in 150 mM Tris-HCl pH 9 solution at 70 °C for 15 min and then incubated with acetone at -20 °C for 20 min. Then, they were blocked (10% goat serum, 0.8 % TritonX, 1% BSA and 1% DMSO in 1X PBS + 0.1% Tween) at 4 °C for 3 h and incubated with active caspase-3 primary antibody (#9661, 1:250, Cell Signaling Technology) diluted in 1% goat serum, 0.8% Triton X-100, 1% BSA in 1X PBS + 0.1% Tween at 4 °C for 3 days. Samples were sequentially washed, and incubated with secondary antibody (#A21244, 1:500, Invitrogen) and Hoechst 33342 (#H3570, 1:100, Invitrogen) in the dark for 2.5 days. After washing, larvae were mounted on glass slides using Aqua/PolyMount (#18606-20, Polysciences, Inc.) and a #1.5 glass coverslip.

3.7.3 Confocal microscopy

All the images were acquired by a Nikon A1 confocal microscope at 40X magnification with 2.5 µm interval Z-stacks. Quantification of active caspase-3 -positive cells was performed using *ImageJ* software by manually counting the immunostained cells present at the different retinal layers in each stack. Each experiment was performed on at least 6 larvae per group, n=3.

3.8 Ocular transcriptomic analysis

3.8.1 RNA extraction

Eye dissection was carried out after 4, 8 and 24 hours of 20 µg/mL CSE or 15 µM atRAL exposure. Before the dissection, larvae were stored in RNAlater® (Merck) at 4 °C overnight. Dissected eyes were homogenized through a 26-gauge needle/syringe and total RNA was extracted using the mirVana™ miRNA Isolation Kit (#AM1561, Invitrogen), according to the manufacturer's instructions. RNA samples were precipitated using 100% ethanol and 3 M sodium acetate solution at −20 °C overnight, then washed with 80% ethanol. Pellets were dissolved in nuclease-free water. The concentration was measured using a Denovix DS-11 spectrophotometer. cDNA was synthesised using the PrimeScript™ RT reagent Kit (Perfect Real Time) (#RR037A, TaKaRa Bio Inc.), according to the manufacturer's protocol. At least 12 larvae were used per experiment.

3.8.2 RT-PCR

A mix containing Power SYBR™ Green PCR Master Mix (#4367659, Applied Biosystems), RNAse-free water and forward and reverse primers (**Table 2**) was prepared on ice and aliquoted in a 384-well plate. 1 µL of cDNA template was added per reaction. Quantitative Real-Time PCR were run using a QuantStudio 7 Flex Real-Time PCR System (Applied Biosystems) under the following conditions: 50 °C for 2 min, 95 °C for 10 min, then 40 cycles at 95 °C for 15 s and 60 °C for 60 s. All experiments were performed in triplicate with three technical replicates. Relative expression of targets was assessed by the $2^{-\Delta\Delta CT}$ method using β-actin as housekeeping gene.

Target	Sequence
Caspase 3a	FW: TAGTGTGTGTGTTGCTCAGTC
	RV: CTCGACAAGCCTGAATAAAG
Nuclear factor erythroid 2–related factor 2	FW: GAGCGGGAGAAATCACACAGAATG
	RV: CAGGAGCTGCATGCACTCATCG
Catalase	FW: TGAGGCTGGGTCATCAGATA
	RV: AAAGACGGAAACAGAAGCGT
Glutathione peroxidase 1a	FW: AGGCACAACAGTCAGGGATT
	RV: CAGGAACGCAAACAGAGGG
β-actin 1	FW: ACATCCGTAAGGACCTG
	RV: GGTCGTTCGTTTGAATCTC

Table 2. Primers for RT-PCR.

3.9 Statistical analysis

All data were reported as the mean ± standard error of the mean (SEM) and analysed on *GraphPad Prism* software. Neurites length was analysed by t-test for unpaired data followed by Kolmogorov-Smirnov's test. Cellular metabolic activity was evaluated by one-way ANOVA followed by Dunnett's or Tukey's multiple comparisons tests. Statistical analysis of OKR data were conducted by Kruskal-Wallis's test followed by Dunn's test or by one-way ANOVA followed by Dunnett's or Tukey's tests or by unpaired t-test with Welch's correction. Statistical analysis of apoptosis was performed by Kruskal-Wallis followed by Dunn's test or by one-way ANOVA using Dunnett's test. VMR data were analysed by Mann-Whitney test or by unpaired t-test with Welch's correction or by Kruskal-Wallis test followed by Dunn's test. Relative gene expression was analysed by one-way ANOVA followed by Dunnett's test. Normal distribution of differences was tested by D'Agostino and Pearson test and significance levels were defined as $p<0.05$ (*), $p<0.01$ (**), $p<0.001$ (***) and $p<0.0001$ (****).

4. RESULTS

4.1 Optimisation of nanoformulated NGF as an eye-targeting drug delivery system

To exploit polyacrylamide nanoparticles as drug delivery system, different reactions were carried out to optimise the ANPs' synthesis (**Table 3**). The protocols mainly differ in polymerization time and presence or absence of argon flux, parameters used to modulate the size distribution of nanoparticles (**MATERIALS AND METHODS, Table 1**). After the assessment of the nanoparticle hydrodynamic diameter and polydispersity index, Alexa Fluor 594-positive ANPs were chosen for the next steps. The selected nanocarrier showed a similar diameter distribution after 10 days post-synthesis, thus suggesting a good stability of the nanoformulation after storage at 4 °C.

Nanoparticles	Functionalisation	Hydrodynamic Diameter	Polydispersity Index	Reaction Time
ANPs	-	6.67 ± 0.89	0.52 ± 0.15	4 h
ANPs	-	11.64 ± 1.19	0.33 ± 0.16	8 h
ANPs	-	575.97 ± 26.37	0.73 ± 0.01	24 h
ANPs	Alexa Fluor 488	17.98 ± 0.56	0.37 ± 0.02	3 h
ANPs	Alexa Fluor 594	13.89 ± 1.74 nm	0.44 ± 0.03	3 h
ANP:PNA	Alexa Fluor 594; PNA	19.97 ± 2.41 nm	0.47 ± 0.09	3 h
ANP:NGF	NGF	n/a	n/a	3 h
ANP:PNA:NGF	Alexa Fluor 594; PNA; NGF	22.81 ± 3.17 nm	0.18 ± 0.03	3 h

Table 3. Nanoparticles characterisation. *Hydrodynamic diameter and polydispersity index of naked and functionalised polyacrylamide nanoparticles. Mean ± SEM, n=3.*

4.1.1 Hydrodynamic diameter and conjugation efficiency evaluations

To improve the applicability of polyacrylamide nanoparticles as nanocarrier for ocular drug delivery, NGF alone or PNA and NGF were conjugated to the nanocarrier through non-covalent functionalisations. To estimate the loading of proteins onto the nanoparticles, BCA and ELISA assays were carried out for quantifying conjugated PNA and NGF, respectively. The PNA binding efficiency was calculated to be around the 62% as the loaded content was 0.62 µg of PNA per µL of particles suspension. The binding efficiency of NGF conjugated to ANPs, as well as to ANP:PNA, was of 37% and 91%, respectively, as the loaded content of proteins was 0.37 µg and 0.91 µg of NGF per µL of particles suspension. Size distribution and polydispersity index of the functionalised nanoparticles were also characterised by DLS measurements (**Figure 7**). ANP:PNA:NGF showed an increase in size distribution (22.81 ± 3.17 nm) compared to PNA-conjugated ANPs (19.97 ± 2.41 nm) and naked ANPs (13.89 ± 1.74 nm)(**Table 3**).

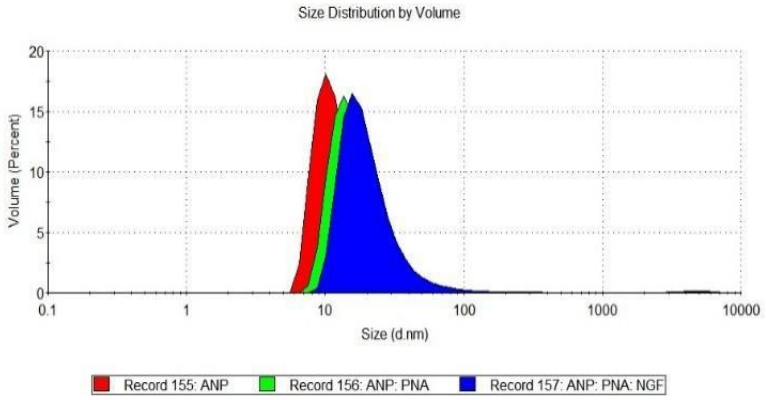

Figure 7. Nanoparticles characterisation through dynamic light scattering measurements. *The increase of hydrodynamic diameter of single- (ANP:PNA, green curve) and double- (ANP:PNA:NGF, blue curve) functionalised polyacrylamide nanoparticles resulted in a shift of size distribution compared to naked ANPs (red curve).*

4.1.2 Ocular distribution profile

To study the localisation of the polymeric unbound nanocarrier and investigate its retinal distribution over time, zebrafish larvae at 3 dpf were IVT injected with ANPs containing the green fluorescent dye Alexa Fluor 488, which were previously obtained by encapsulation of Alexa Fluor 488 dye into the polymeric matrix of nanoparticles during their synthesis carried out by radical polymerization. Injected larvae were then fixed at 4, 8 and 24 hpi, cryosectioned, and imaged in DAPI and FITC channels (**Figure 8A**). By analysing cross-sections at different time points, a different profile of particles distribution through the retinal layers has been

observed over time. At 4 hpi, green fluorescent spots, corresponding to Alexa Fluor 488-positive ANPs, were found to localise at both the GCL and INL. At 8 hpi, they were also observed at the PRs and the RPE layers, where the Alexa Fluor 488 signal was mainly present at 24 hpi and no particles were found at the GCL, thus suggesting their spontaneous migration through the retinal layers over time (**Figure 8B**).

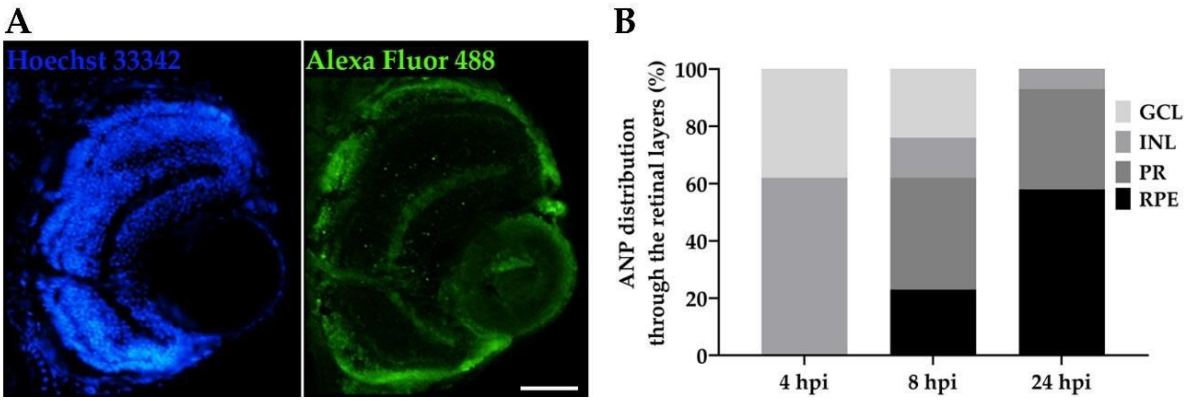

Figure 8. Nanoparticles distribute through retinal layers after intravitreal injection in zebrafish larvae. A) *Representative images of a retinal cross-section of a zebrafish larva IVT injected with Alexa Fluor 488-positive polyacrylamide nanoparticles, analysed at 4 hours post-injection (hpi). Hoechst staining allows to distinguish the retinal layers. In FITC channel, the intense green spots clearly highlight the presence of Alexa Fluor 488-positive nanoparticles in the injected eye.* ***B)*** *Quantitative evaluation of the distribution of Alexa Fluor 488-positive polyacrylamide nanoparticles in the retinal layers at different time points. n=15 injected eyes from three independent experiments. GCL, Ganglion Cell Layer; INL, Inner Nuclear Layer; PRs, photoreceptors; RPE, Retinal Pigment Epithelium. Scale bar: 50 µm.*

Interestingly, no ANPs were found at the right eye used as not-injected control (**Figure 9**).

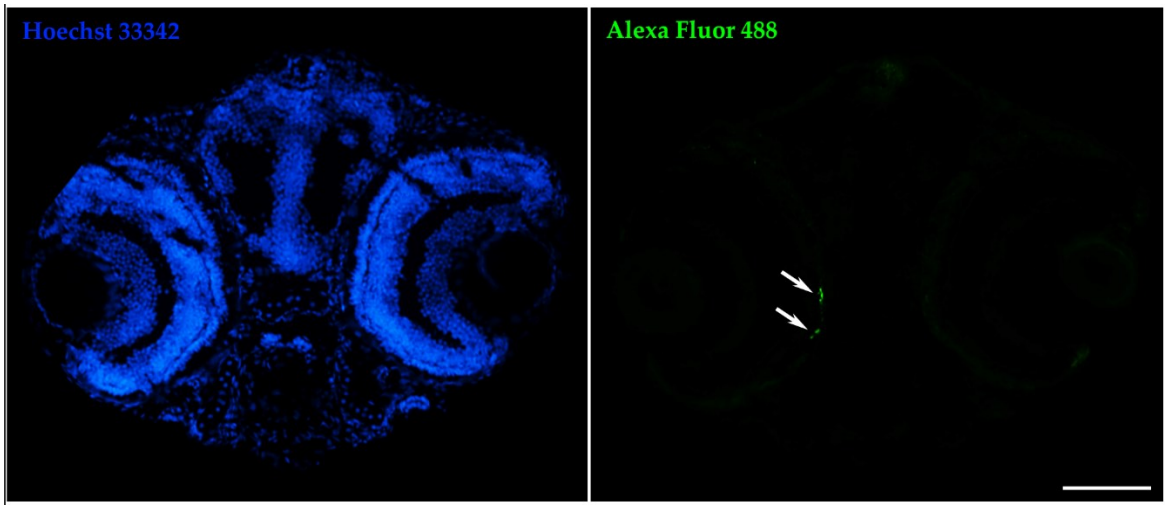

Figure 9. Nanoparticles do not diffuse in the contralateral eye after intravitreal injections. *Representative images of a retinal cross-section of a zebrafish larva IVT injected with Alexa Fluor 488-positive polyacrylamide nanoparticles, analysed at 24 hours post-injection (hpi). Cell nuclei stained with*

Hoechst 33342 (blue); retinal distribution of nanoparticles revealed by the fluorescent dye Alexa Fluor 488 (green). Scale bar: 200 µm.

Nevertheless, preliminary *in vivo* whole-mount imaging suggested the presence of green fluorescent ANPs not only in the injected eye, but also at the pronephros, where they were found to accumulate already at 4 hpi, thus indicating that the nanocarrier was not stably retained in the ocular environment (**Figure 10**).

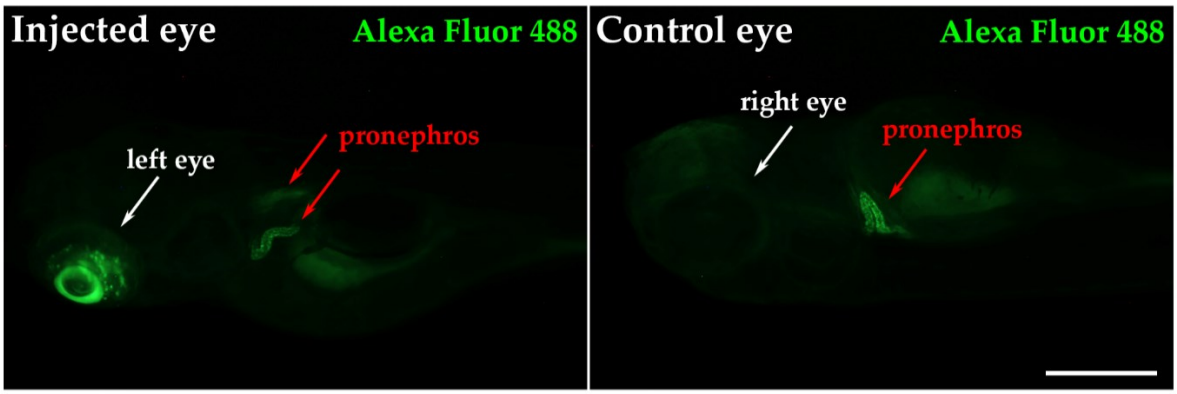

Figure 10. Naked polyacrylamide nanoparticles accumulate in the pronephros after intravitreal injections*. Representative images of a zebrafish larva IVT injected with Alexa Fluor 488-positive polyacrylamide nanoparticles, analysed at 4 hpi. Alexa Fluor 488-positive ANPs (green) were observed in both injected left eye and pronephros. No fluorescence was detected in the uninjected right eye used as control. Scale bar: 300 µm.*

To confirm that the PNA conjugation enhances the ANPs capability to target the ocular posterior segment, nanoparticles containing a red fluorescent Alexa Fluor 594 dye were functionalised with a FITC-conjugated PNA (ANP:PNA) in order to identify the distribution profile of the carrier (red fluorescent ANPs) and the cargo (green fluorescent PNA). Naked and PNA-conjugated ANPs were IVT injected in 3 dpf larvae and the fluorescence was checked after 4 and 24 hpi (**Figure 11**). After 4 hpi, a strong red fluorescent signal was observed in the left eye of both injected groups. However, only the naked ANPs-injected larvae, showed the presence of nanoparticles at the level of the pronephros at 24 hpi, confirming the evidence previously described and suggesting their instability in the ocular environment. On the contrary, the PNA-conjugated ANPs were stably retained in the injected eye until 24 hpi, as shown by the presence of green fluorescence of the FITC-conjugated PNA in the left eye at all the time points and its absence in any other tissue of the larvae, thus suggesting a crucial improvement of the polymeric nanoformulation as ocular drug delivery nanocarrier. These profiles were observed in 100% of the injected larvae. No fluorescence was found in control larvae injected with saline, as expected (**Figure 11**).

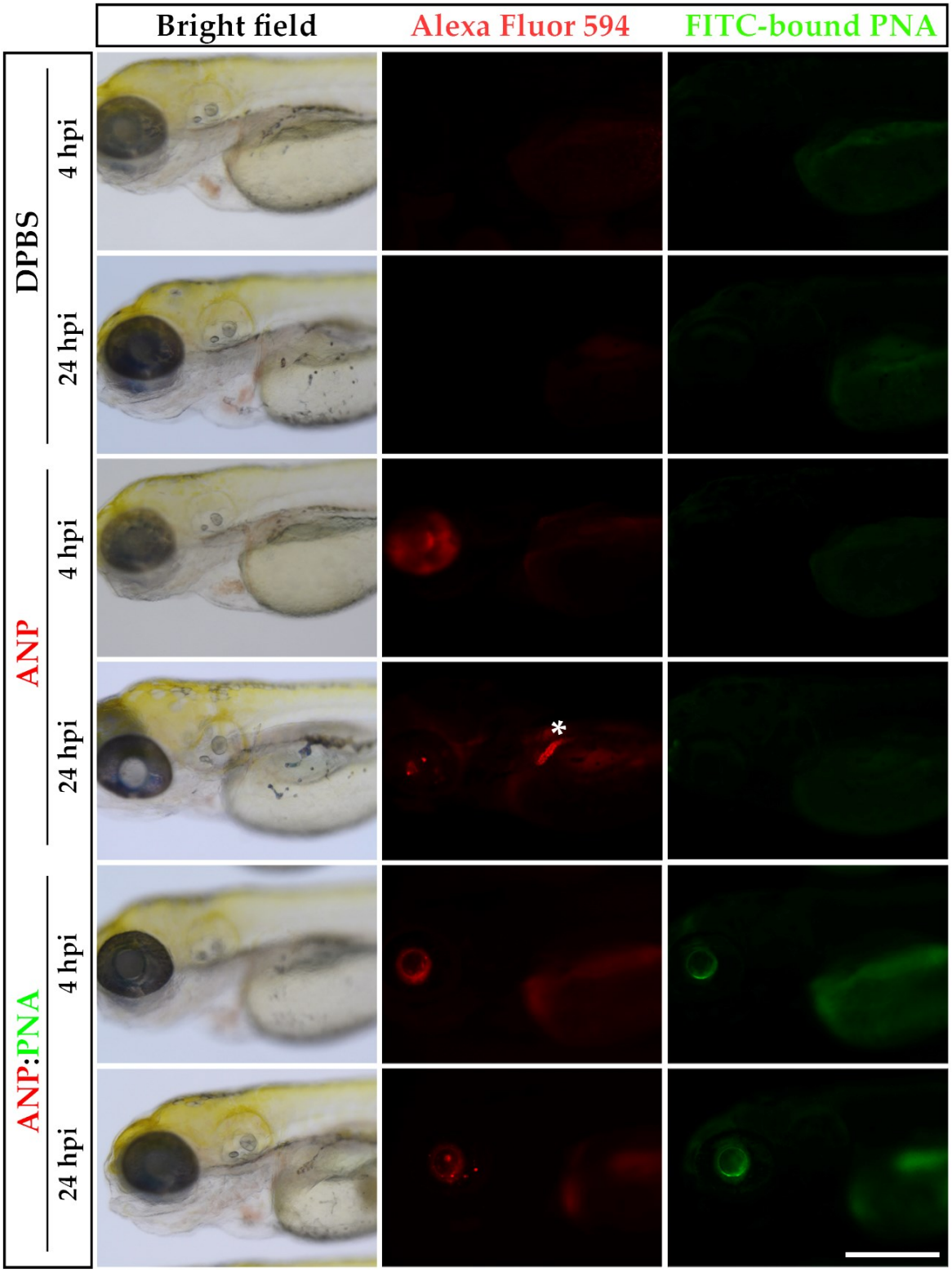

Figure 11. Prolonged localisation of nanoparticles at the site of injection. *Representative images of larvae at 3 dpf IVT injected with naked Alexa Fluor 594-positive nanoparticles (ANPs) or FITC-labelled PNA-conjugated polyacrylamide nanoparticles (ANP:PNA), analysed at 4 and 24 hours post-injection (hpi). As control, zebrafish larvae were IVT injected with DPBS. White asterisk indicates the pronephros. n=45 injected eyes from three independent experiments. Scale bar: 300 µm.*

4.1.3 NGF-conjugated nanoparticles bioactivity

To assess the biological activity of ANPs- and ANP:PNA-conjugated NGF, pheochromocytoma PC12 cells were used to perform an *in vitro* test. In fact, PC12 cells differentiate in a neuron-like phenotype in response to the NGF treatment. The presence of neurites after 4 days of treatment in both free and conjugated-NGF groups suggested that NGF confirmed its biological activity by triggering the neurites formation. On the contrary, untreated and ANP:PNA-treated cells maintained the round-shape morphology. Additionally, the neurites length was comparable between cells treated with free NGF (127.5 ± 4.17 μm), ANP:NGF (75.08 ± 3.23 μm) and ANP:PNA:NGF (129 ± 3.74 μm), thus confirming that the functionalisation processes do not affect the biological properties of the NGF (**Figure 12**). Controls data were not included as no neurite formation occurred in both untreated and ANP:PNA-treated groups (**Figure 12**).

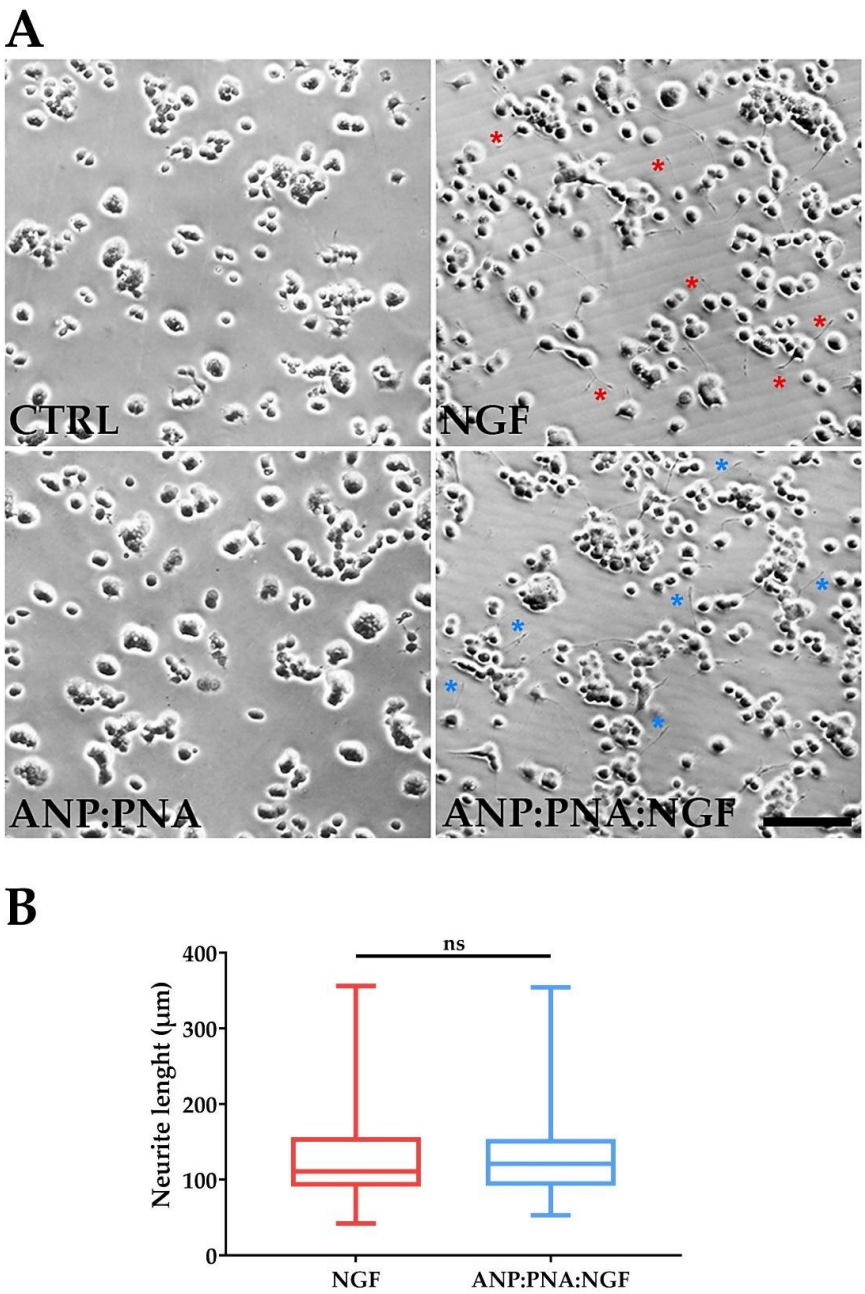

Figure 12. NGF exerts its biological activity upon nanoformulation. A*) Representative images of PC12 cells incubated for 4 days with 100 ng/mL of free NGF or with the same concentration of NGF bound to PNA-conjugated polyacrylamide nanoparticles (ANP:PNA:NGF). As control, PC12 cells were incubated with PNA-conjugated nanoparticles (ANP:PNA) or DPBS. Asterisks indicate the formation of neurites. Scale bar: 300 µm.* ***B****) Quantitative evaluation of neurite length in PC12 cells incubated with NGF or ANP:NGF or ANP:PNA:NGF. n=180 neurites from three biological replicates. Data analysed by t-test for unpaired data followed by Kolmogorov-Smirnov test. ns, p>0.05.*

4.2 Models of oxidative damage

4.2.1 Effects of hydrogen peroxide on ARPE-19 cellular metabolic activity

To establish the concentration of hydrogen peroxide able to reduce cellular metabolic activity of human RPE cells, different concentrations were tested for 24 h, then an MTT assay was performed. Data showed that the treatment with 300, 350, 400 and 600 µM H_2O_2 significantly reduced the metabolic activity of treated cells compared to the untreated control group (***, p=0.0008 and ****, p<0.0001), while no cytotoxic effect emerged by using lower concentrations of H_2O_2 (200 and 250 µM H_2O_2, ns, p>0.05) (**Figure 13**). As 300 µM H_2O_2 was the minimum concentration altering the percentage of cellular metabolic activity, which was used as an indicator of cell viability, it was selected to reproduce an oxidative condition in further experiments.

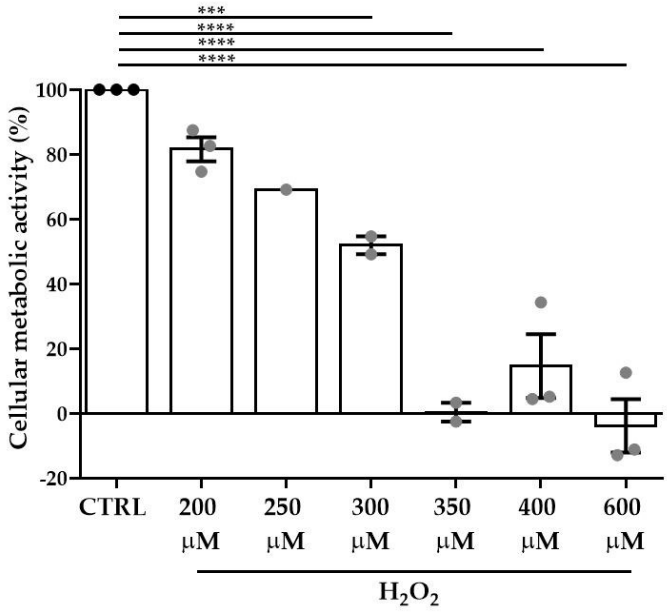

Figure 13. Hydrogen peroxide reduce cellular metabolic activity of human RPE cells in dose-dependent manner*. Induction of an oxidative condition in ARPE-19 cell line using increasing concentration of H_2O_2 for 24 hours. MTT assay was performed to evaluate cellular metabolic activity as an indicator of cell viability. Absorbance values of all the groups were normalised to those of the untreated control sample (CTRL), which was set at 100%. n≥1 independent experiments. Statistical analysis carried out by one-way ANOVA applying Dunnett's multiple comparisons test. ns, p>0.05; ***, p<0.001; ****, p<0.0001.*

4.2.2 Assessment of nanoformulated NGF protection in ARPE-19 cells

To validate the neuroprotective effect of our NGF-based nanoformulation, human retinal pigment epithelial ARPE-19 cells were incubated with hydrogen peroxide to mimic an oxidative condition as occurring in retinal degeneration (**Figure 14**). Cellular metabolic activity was assessed by MTT assay after 24 h of co-incubation of cells with H_2O_2 and NGF-conjugated nanoparticles or free NGF. As expected, data showed a cytotoxic effect in the H_2O_2-treated group compared to the untreated control (****, $p<0.0001$) as oxidative damage arose. While free neurotrophin was not able to counteract H_2O_2-induced cell mortality, cellular metabolic activity was preserved by nanoformulated NGF (ANP:PNA:NGF) compared to H_2O_2-treated group (****, $p<0.0001$), thus suggesting a pronounced protective effect of NGF when nanoformulated.

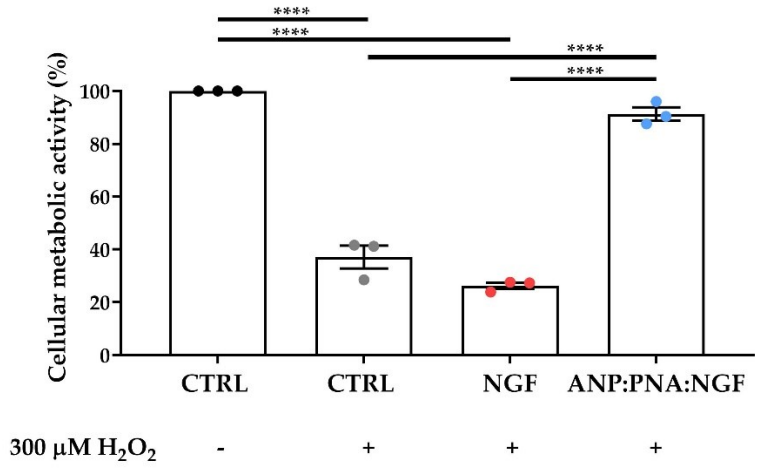

Figure 14. Nanoformulated NGF exerts a protective effect on human RPE cells against oxidative stress. *ARPE-19 cells were co-treated with 100 ng/mL of free NGF (NGF) or nanoformulated NGF (ANP:PNA:NGF) and 300 μM H_2O_2 for 24 hours. MTT assay was performed to evaluate cellular metabolic activity. Absorbance values of all the groups were normalised to those of the untreated control sample (CTRL), which was set at 100%. n=3 biological replicates. Statistical analysis carried out by one-way ANOVA applying Tukey's multiple comparisons test. ****, $p<0.0001$.*

4.2.3 Neuroprotective impact of nanoformulated NGF on visual behaviour in zebrafish

To further confirm the neuroprotective activity of the ANP:PNA-conjugated NGF, *in vivo* experiments resembling a condition of retinal degeneration were performed in zebrafish larvae, by inducing a retinal oxidative damage as previously developed by our research group [90]. Free NGF or nanoformulated neurotrophin (ANP:NGF or ANP:PNA:NGF) was IVT injected

as a preventive treatment against an oxidative injury obtained through the IVT injection of hydrogen peroxide. To evaluate the effect of nanoformulated neurotrophin in preventing vision impairment, visual function of injected larvae was evaluated by optokinetic response (OKR) assay.

Data showed a statistically significant reduction (****, $p<0.0001$) in the ocular movements (saccades) recorded in the larvae injected with H_2O_2 (4.64 ± 0.51 saccades per minute) compared to the negative control group (9.42 ± 0.63 saccades per minute), thus confirming a visual impairment of larvae exposed to oxidative stress. The preventive injection of the free NGF (5.81 ± 0.49 saccades per minute) or ANPs-conjugated neurotrophin (5.1 ± 0.93 saccades per minute) was not able to prevent the visual dysfunction induced by the hydrogen peroxide (ns, $p>0.05$). Moreover, larvae pre-treated with free or ANPs-conjugated NGF showed a significantly lower number of saccades than the negative control (***, $p=0.0006$ and **, $p=0.0039$, respectively). Conversely, the number of saccades of ANP:PNA:NGF-injected larvae (8.59 ± 0.69 saccades per minute) was significantly higher than that recorded in larvae treated with only H_2O_2 (***, $p=0.0002$). Interestingly, ANP:PNA:NGF-pre-treated larvae displayed a significant increase of ocular movements also in comparison to free NGF and ANPs-conjugated NGF larvae (*, $p=0.031$ and *, $p=0.039$, respectively), thus suggesting a neuroprotective effect of NGF only when nanoformulated with the PNA-conjugated nanoparticles (**Figure 15**).

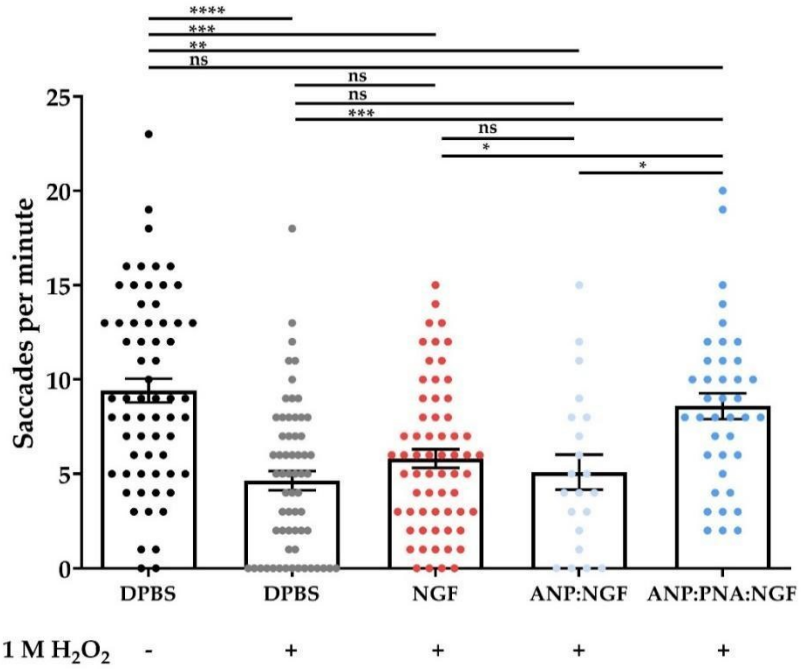

Figure 15. ANP:PNA-formulated NGF improves visual function impaired by oxidative stress in zebrafish larvae. *Evaluation of visual function by OKR assay in zebrafish larvae pre-injected with 1 ng of free or ANPs-conjugated or ANP:PNA-conjugated NGF (or DPBS as control) and exposed to oxidative stress through the IVT injection of 1 M H_2O_2. Negative controls were IVT injected with DPBS twice. n≥21 larvae*

*for each group from 4 biological replicates. Statistical analysis carried out by Kruskal-Wallis test followed by Dunn's multiple comparisons test. ns, p>0.05; *, p<0.01; **, p<0.01; ***, p<0.001 and ****, p<0.0001.*

4.2.4 Neuroprotective effect of nanoformulated NGF against retinal cell apoptosis

To study the mechanism underlying the recovery of compromised visual function induced by hydrogen peroxide exposure, the neuroprotective effect of NGF-conjugated nanoparticles was investigated at a functional level. Both TUNEL assay and immunohistochemistry for the detection of active caspase 3 positive cells were performed to study apoptosis, as a consequence of an oxidative stress condition [90,97].

TUNEL assay was performed on retinal sections. The number of apoptotic cells resulted significantly higher (**, p=0.003) in the retina of H_2O_2-treated group (8.36 ± 0.97 TUNEL-positive cells) compared to the saline-injected control (0.25 ± 0.25 TUNEL-positive cells). In relation to the preventive injection with free or nanoformulated NGF, a statistical significant reduction of apoptotic cells was observed in ANP:PNA:NGF-pre-treated group (*, p=0.02) compared to H_2O_2 control group, while no significant changes were observed in NGF-pre-treated larvae compared to H_2O_2-injected controls (ns, p>0.05). Indeed, ANP:PNA:NGF-pre-treated larvae showed 1.50 ± 0.96 TUNEL-positive cells, while NGF pre-treated larvae showed 4.63 ± 1.03 TUNEL-positive cells (**Figure 16**).

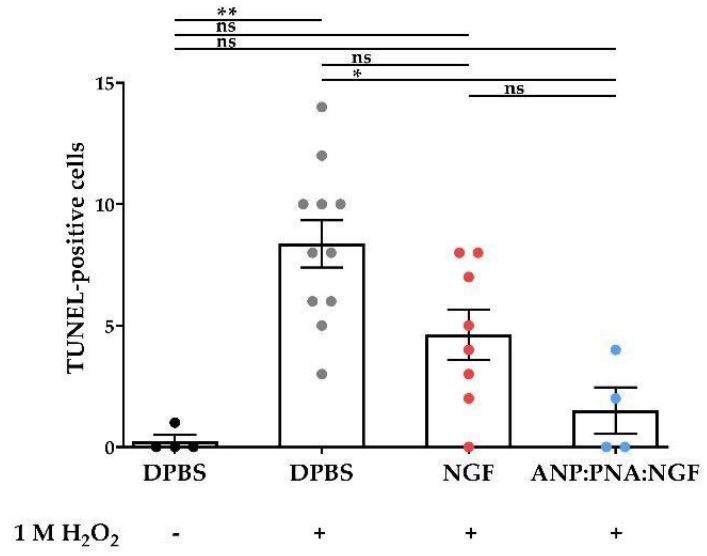

Figure 16. Preventive IVT injection of nanoformulated NGF results in a significant reduction of apoptotic cells in the retina of zebrafish larvae after an oxidative damage induced by ocular administration of H_2O_2. *Quantitative evaluation of apoptosis through the detection of TUNEL-positive cells in the retina of zebrafish larvae pre-injected with 1 ng of free or ANP:PNA-conjugated NGF (or DPBS*

*as control) and exposed to oxidative stress through the IVT injection of 1 M H_2O_2. Negative controls were IVT injected with DPBS twice. n≥4 larvae for each group from one biological replicate. Statistical analysis carried out by Kruskal-Wallis followed by Dunn's multiple comparisons test. ns, p>0.05; *, p<0.05 and **, p<0.01.*

To analyse in depth the apoptotic event occurring in the retina after the exposure to hydrogen peroxide-induced oxidative stress, whole-mount immunostaining of the active caspase 3 was carried out. According to the OKR data, the number of apoptotic cells resulted significatively higher (***, p=0.0003) in the H_2O_2-treated group (20.8 ± 4.4 positive cells) compared to the negative control (6.2 ± 0.9 positive cells), hence corroborating a cytotoxic damage induced by the injection of the hydrogen peroxide. Interestingly, the reduction of apoptotic cells in the retina (*, p=0.011) was only observed in the H_2O_2-injected larvae pre-treated with ANP:PNA:NGF (9.7 ± 2.02 positive cells) while no neuroprotection was observed in the larvae pre-treated with the free neurotrophin (13.8 ± 2.32 positive cells), since the number of apoptotic cells was not statistically different to the group exposed to H_2O_2 (ns, p>0.05) (**Figure 17**). These data are in line with the visual impairment revealed by the optokinetic response assay and show a promising effect of our neuroprotective NGF-based nanoformulation against the retinal degeneration induced by oxidative stress.

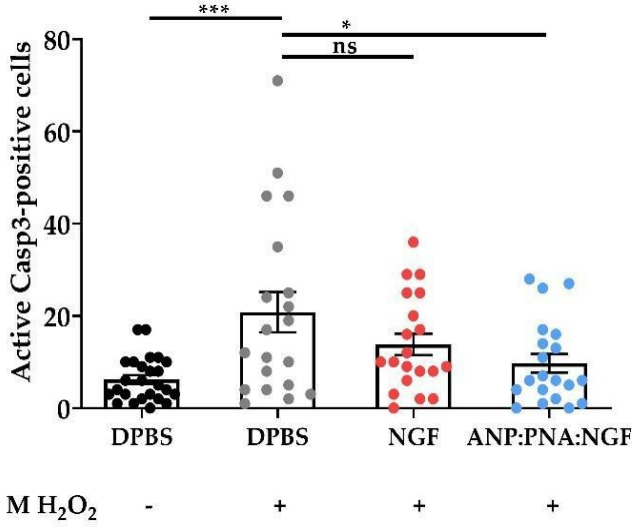

Figure 17. Nanoformulated NGF protects retinal cells from oxidative stress-triggered apoptosis in the eye of zebrafish larvae. *Quantitative evaluation of apoptosis through the detection of active caspase 3-positive cells by immunofluorescence in the retina of zebrafish larvae pre-injected with 1 ng of free or ANP:PNA-conjugated NGF (or DPBS as control) and exposed to oxidative stress through the IVT injection of 1 M H_2O_2. Negative controls were IVT injected with DPBS twice. n≥20 larvae for each group from three biological replicates. Data analysed by one-way ANOVA using Dunnett's multiple comparisons test. ns, p>0.05; *, p<0.01 and ***, p<0.001.*

4.3 Evaluation of cigarette smoke extract-triggered visual impairment

To study the effect of CSE exposure on visual function, zebrafish larvae at 4 dpf were exposed to 20 and 25 µg/mL of extract solution for 24 h, followed by the evaluation of the optokinetic response. Larvae immersed in 0.05% DMSO solution were used as a control. Data showed that the number of saccades of groups treated with 20 and 25 µg/mL CSE (17.78 ± 2.047 and 17.20 ± 1.705 saccades per minute, respectively) was significantly lower (***, p=0.0001 and ****, p<0.0001, respectively) compared to the negative control group (30.98 ± 2.037 saccades per minute) (**Figure 18**).

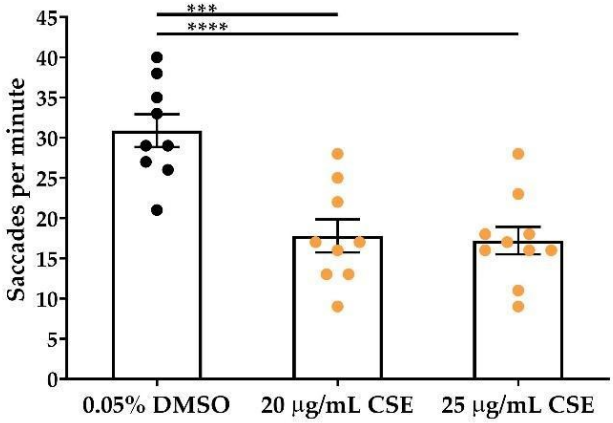

Figure 18. Exposure to cigarette smoke extract (CSE) negatively affects visual function of zebrafish larvae. *Evaluation of visual function by OKR assay in zebrafish larvae exposed to different concentrations of CSE for 24 h. Larvae treated with 0.05% DMSO vehicle solution were used as controls. n≥9 larvae for each group from one biological replicate. Data analysed by one-way ANOVA followed by Dunnett's multiple comparisons test. ***, p<0.001 and ****, p<0.0001.*

Therefore, further experiments were carried out by using 20 µg/mL CSE as minimum concentration able to establish a condition of visual impairment, as confirmed by the statistically significant difference (****, p<0.0001) in the number of saccades recorded in the CSE-treated larvae (15.53 ± 1.191) and in the DMSO-control group (25.41 ± 1.175) after 24 h of exposure (**Figure 19**). Additionally, only the 20% of 20 µg/mL CSE-treated larvae showed deflated swim bladder compared to 60% of malformation observed after exposure to the higher dose 25 µg/mL CSE. Normal morphology was observed in the controls, as expected.

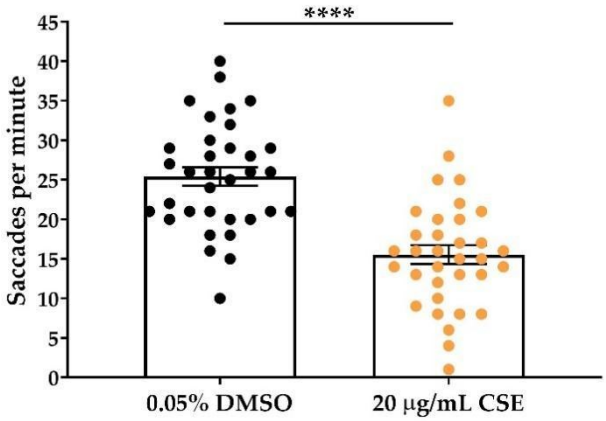

Figure 19. Exposure to cigarette smoke extract (CSE) strongly impairs visual function of zebrafish larvae. *Evaluation of visual function by OKR assay in zebrafish larvae exposed to 20 μg/mL CSE for 24 h. Larvae treated with 0.05% DMSO vehicle solution were used as controls. n=34 larvae/group from three biological replicates. Data analysed by unpaired t-test with Welch's correction. ****, p<0.0001.*

To extend the investigation of the effect of CSE on visual modulation, visual motor response was studied after 24 h of CSE treatment for evaluating the activity of larvae in response to sudden light changes. Data showed that the average overall locomotor activity of CSE-treated larvae (0.011 ± 0.001 ms/s) was significantly reduced (****, $p<0.0001$) compared to the control group (0.021 ± 0.001 ms/s). No differences (ns, $p>0.05$) were found in the average maximum peak activity of CSE-treated larvae (0.104 ± 0.01 ms/s) compared to the control group (0.123 ± 0.009 ms/s) when the light went OFF. However, a significative reduction (*, $p=0.034$) of the average maximum ON peak activity was recorded in CSE-treated larvae (0.05 ± 0.01 ms/s) compared to the control group (0.09 ± 0.01 ms/s) (**Figure 20**).

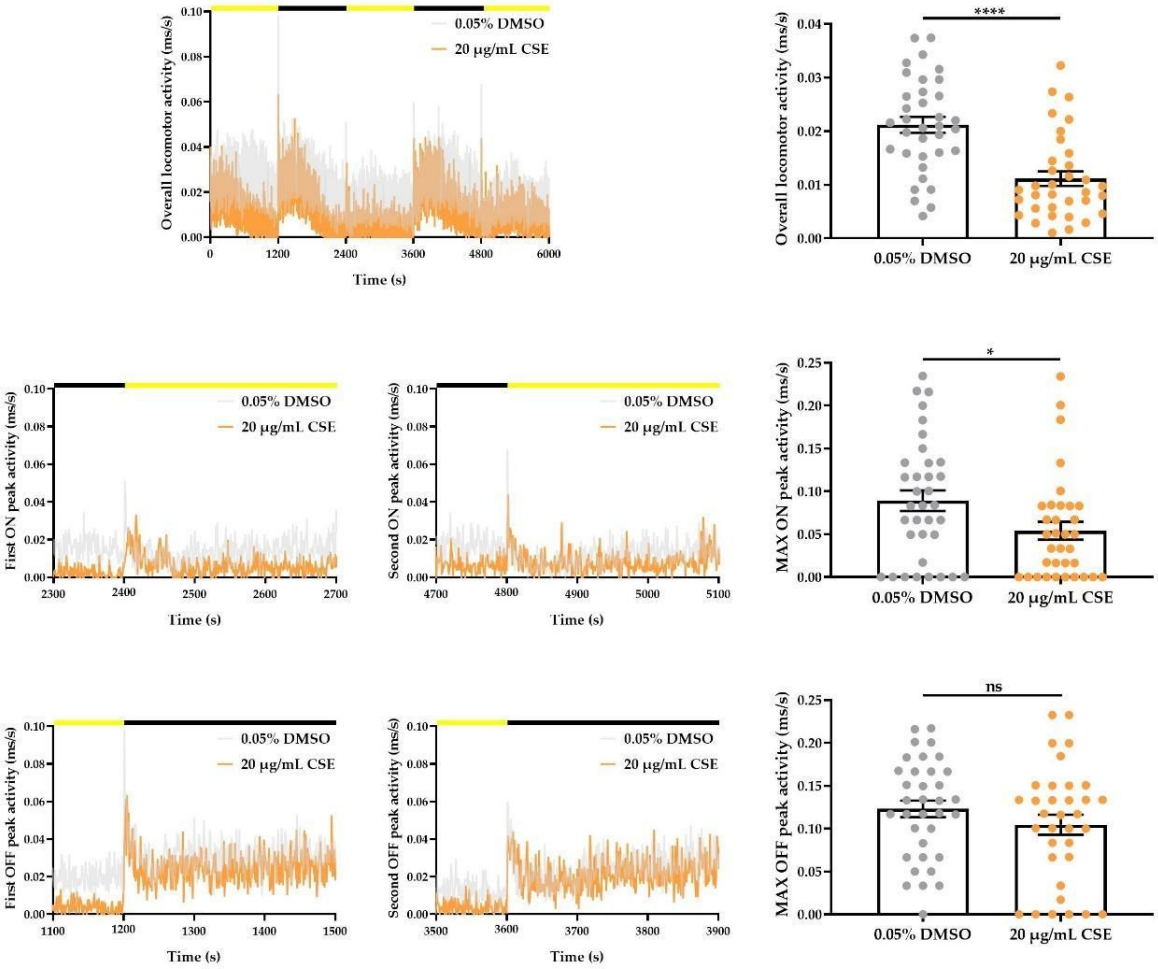

Figure 20. Exposure to cigarette smoke extract (CSE) causes a reduction of locomotor activity of zebrafish larvae*. Traces showing overall locomotor activity and maximum ON and OFF peaks activities evaluated by VMR assay in zebrafish larvae exposed to 20 µg/mL CSE for 24 h. Larvae treated with 0.05% DMSO vehicle solution were used as controls. n≥34 larvae/group from three biological replicates. Statistical analysis carried out by unpaired t-test with Welch's correction and Mann Whitney test. ns, p>0.05; *, p<0.05 and ****, p<0.0001.*

4.3.1 Transcriptomic profile of oxidative stress biomarkers

To investigate the effect of short-term CSE exposure in the eye of zebrafish larvae, relative expression of antioxidant genes, including catalase (*cat*) and glutathione peroxidase 1 (*gpx1a*), as well as nuclear factor erythroid 2-related factor 2 (*nfe2l2a*), as a key regulator of cellular response against oxidative stress, and *casp3a* as an indicator of apoptosis was analysed by RT-PCR after 4 and 24 h of CSE exposure. No significant differences in *cat*, *nfe2l2a* and *casp3a* expression were observed CSE-treated larvae compared to the controls (ns, p>0.05), at both time points of 4 and 24 h. Interestingly, a significantly higher expression of *gpx1a* transcript in

the eye of larvae treated with CSE for 4 (****, p<0.0001) and 24 h (***, p=0.0003) was observed with respect to 0.05% DMSO control larvae (**Figure 21**).

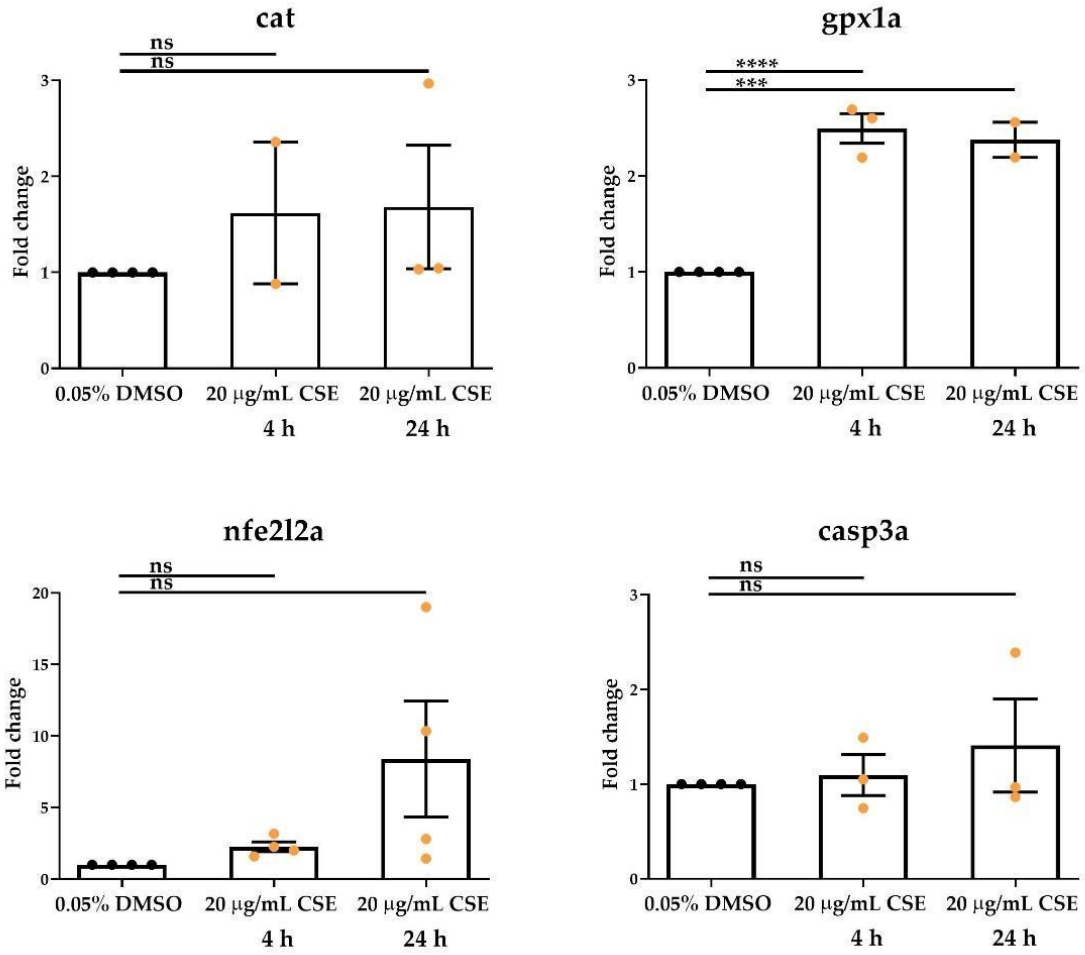

Figure 21. Exposure to cigarette smoke extract (CSE) results in a significant increased expression of glutathione peroxidase 1 (gpx1a) in the eye of zebrafish larvae. *RT-PCR analysis of oxidative stress-associated genes (cat, gpx1a, nfe2l2a* and *casp3a) revealed an increased expression of gpx1a in the eye of zebrafish larvae after 4 and 24 h of 20 µg/mL CSE exposure compared to 0.05% DMSO control group. n≥48 larval eyes/group from n≥2 biological replicates. Statistical analysis carried out by one-way ANOVA followed by Dunnett's multiple comparison test. Data normalized to β-actin expression and 0.05% DMSO solution-treated group.*

4.3.2 Efficacy assessment of nanoformulated NGF preventive treatment

The efficacy of NGF-based nanocarrier was assessed as preventive treatment against the visual impairment induced by CSE. Therefore, IVT injections of free or nanoformulated NGF were performed 16 h prior to the exposure to 20 μg/mL CSE, and visual function of 5 dpf larvae were studied by OKR assay. The number of saccades recorded in the negative vehicle control (28.44 ± 1.13 saccades per minute) was significantly higher (****, p<0.0001) compared to the CSE-treated positive control group (13.68 ± 0.98 saccades per minute), in line with the data reported in the literature (*manuscript under review*). Preventive injections of free NGF (21.96 ± 1.09 saccades per minute) or its nanoformulation ANP:PNA:NGF (20.19 ± 1.33 saccades per minute) significantly improved visual function impaired by exposure to the CSE (****, p<0.0001 and ***, p=0.0004, respectively) (**Figure 22**). This rescue was only partial since there was still a significant difference compared to the negative control group (**, p=0.0017 and ****, p<0.0001, respectively).

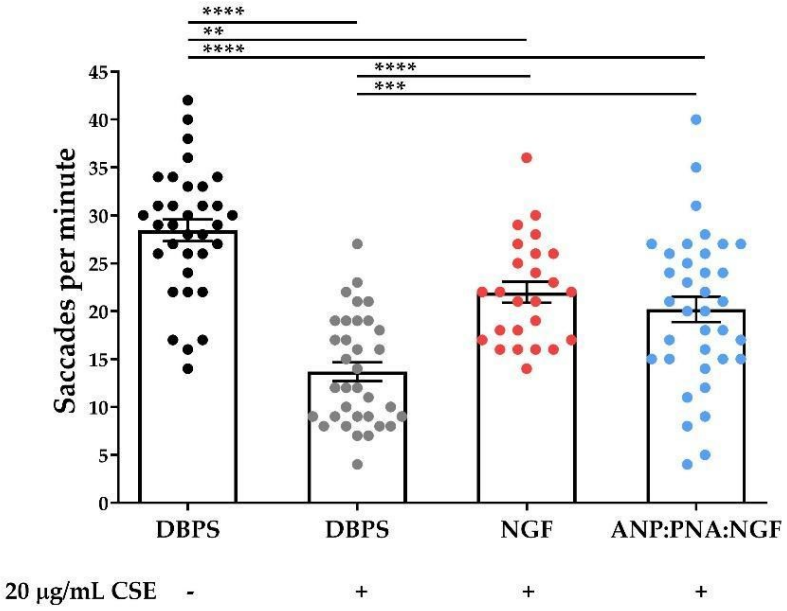

Figure 22. Intravitreal injection of ANP:PNA-conjugated NGF attenuates cigarette smoke extract (CSE)-induced visual impairment in zebrafish larvae. *Evaluation of visual function by OKR assay in zebrafish larvae pre-treated with free or nanoformulated NGF and exposed to CSE. Negative control group was IVT injected with DPBS and treated with 0.05% DMSO solution. n≥25 larvae for each group from three biological replicates. Statistical analysis carried out by one-way ANOVA followed by Tukey's multiple comparisons test. **, p<0.01; ***, p<0.001; ****, p<0.0001.*

The visual behaviour of zebrafish larvae pre-treated with free or nanoformulated NGF and exposed to 20 µg/mL CSE was additionally investigated through VMR assay, in accordance with the protocol previously described. The overall locomotor activity of the negative control group (injected with DPBS and treated with vehicle) was significantly higher compared to both positive control (injected with DPBS and exposed to CSE) and larvae pre-treated with NGF (*, p=0.01 and p=0.0109, respectively). Indeed, DMSO-treated larvae showed an average overall locomotor activity of 0.016 ± 0.0024 ms/s, versus the CSE-treated and NGF pre-treated larvae, which showed 0.007 ± 0.0017 ms/s and 0.007 ± 0.0016 ms/s average overall activity, respectively. No difference (ns, p>0.05) emerged in the larvae pre-treated with nanoformulated NGF, which displayed 0.011 ± 0.0023 ms/s average activity, compared to the negative control group. However, neither free and ANP:PNA-conjugated NGF pre-treated larvae showed an improved overall locomotory activity compared to the positive control group (ns, p>0.05) (**Figure 23**).

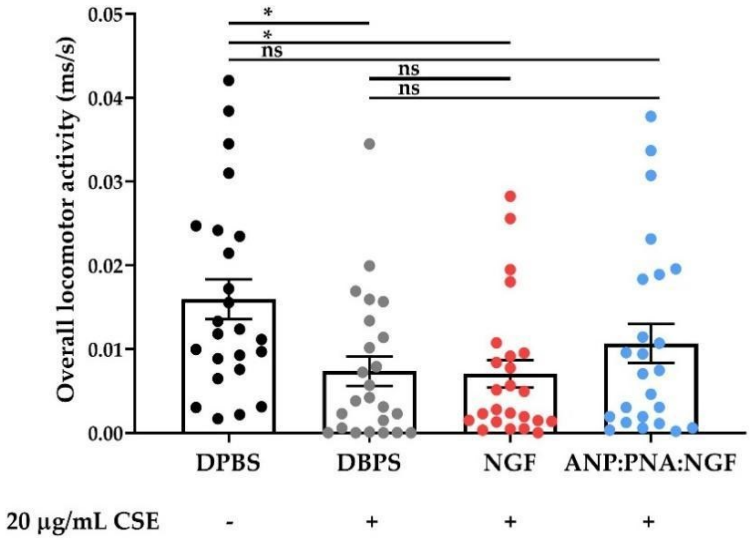

Figure 23. Preventive injection of ANP:PNA-conjugated NGF results in a positive trend of locomotor activity in zebrafish larvae exposed to CSE. *Evaluation of average overall locomotor activity of zebrafish larvae pre-treated with free or nanoformulated NGF and exposed to CSE. Larvae injected with DPBS and treated with 0.05% DMSO vehicle solution were used as controls. n=24 larvae for each group from two biological replicates. Data analysed by Kruskal-Wallis test followed by Dunn's multiple comparisons test. ns, p>0.05; *, p<0.05.*

4.4 Evaluation of all-*trans* retinal-induced visual impairment

All-*trans* retinal (atRAL) is a highly reactive vitamin A aldehyde produced during the visual cycle, and the alteration of its clearance leads to retinal degeneration [98]. To study the modulation of exogenous administration of atRAL on visual behaviour, zebrafish larvae at 4 dpf were exposed to a solution containing the compound at the concentration of 15 µM. This concentration was selected after a dose-response assay in zebrafish larvae, aiming to identify an alteration on vision (data not shown). Larvae immersed in 0.05% DMSO solution were used as control. As before, visual functions were firstly assessed by evaluating the optokinetic response. Data showed that the number of ocular movements of atRAL-treated larvae (8.5 ± 1.31 saccades per minute) was significantly lower than the DMSO vehicle control (23.40 ± 1.11 saccades per minute; ****, $p<0.0001$), thus suggesting an impairment of visual function induced by the exposure to atRAL (**Figure 24**). Additionally, the 36% of 15 µM atRAL-treated larvae showed deflated swim bladder, while no alterations were observed in the vehicle-treated larvae.

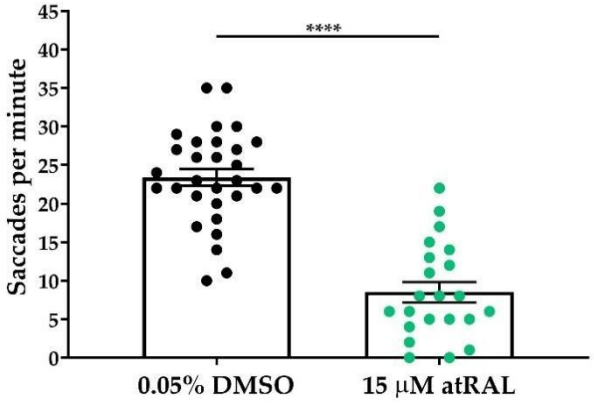

Figure 24. Exposure to all-trans retinal (atRAL) strongly reduces visual function of zebrafish larvae. *Evaluation of visual function by OKR assay in zebrafish larvae exposed to 15 µM atRAL for 24 h. Larvae treated with 0.05% DMSO vehicle solution were used as controls. n≥22 larvae for each group from three biological replicates. Data analysed by unpaired t-test with Welch's correction. ****, $p<0.0001$.*

VMR assay was carried out to investigate the behaviour of larvae treated with 15 µM atRAL in response to light changes. After 24 h of exposure, the overall locomotor activity and the maximum peak activities during ON and OFF light chances were analysed. A trend of reduction in the average overall locomotor activity was observed in larvae treated with atRAL (0.017 ± 0.002 ms/s) compared to control group (0.021 ± 0.001 ms/s), although the difference was not statistically significant (ns, $p>0.05$). In relation to the average maximum activity at the light

changes, no significant reductions were observed between control and atRAL-treated larvae (ns, p>0.05). The average maximum peak ON activity was 0.09 ± 0.01 ms/s for the negative control group and 0.11 ± 0.01 ms/s for the atRAL-treated group, while the average maximum peak OFF activity was 0.12 ± 0.01 ms/s and 0.11 ± 0.02 ms/s, respectively (**Figure 25**).

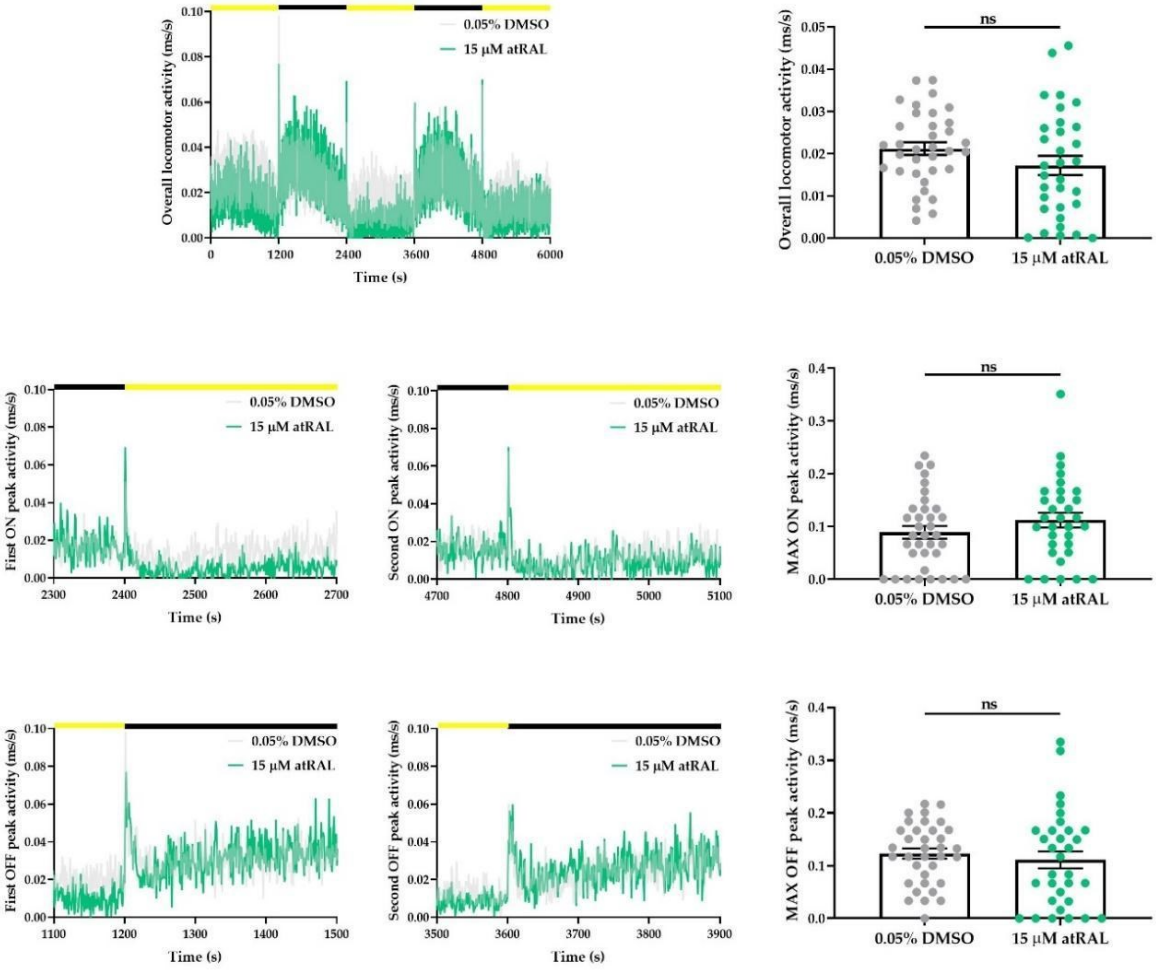

Figure 25. Exposure to all-trans retinal (atRAL) does not affect the locomotor activity of zebrafish larvae. *Traces showing overall locomotor activity and maximum ON and OFF peaks activities evaluated by VMR assay in zebrafish larvae exposed to 15 µM atRAL for 24 h. Larvae treated with 0.05% DMSO vehicle solution were used as controls. n≥32 larvae/group from three biological replicates. Statistical analysis carried out by unpaired t-test with Welch's correction. ns, p>0.05.*

4.4.1 Differential gene expression of oxidative stress biomarkers

To investigate the effect of short-term atRAL exposure in the eye of zebrafish larvae, relative expression of catalase (*cat*), glutathione peroxidase 1 (*gpx1a*), nuclear factor erythroid 2–related factor 2 (*nfe2l2a*) and caspase 3 (*casp3a*) was analysed by RT-PCR after 4 and 24 h of exogenous administration of atRAL. No significant differences in *cat*, *gpx1a*, *nfe2l2a* and *casp3a* expression were observed in both 4 and 24 h atRAL-treated larvae compared to 0.05% DMSO control larvae (ns, p>0.05) (**Figure 26**).

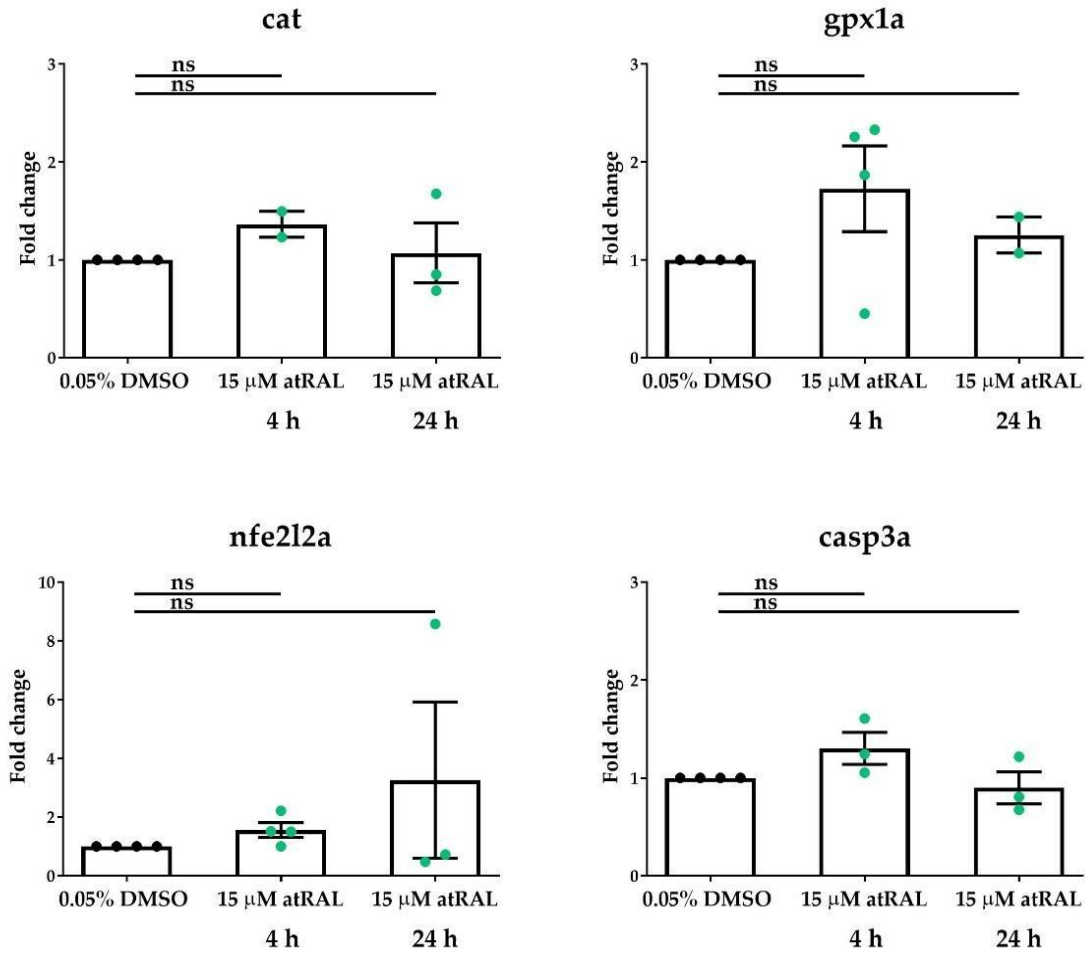

Figure 26. Exposure to all-trans retinal (atRAL) does not induce changes in the relative expression of oxidative stress-associated genes in the eye of zebrafish larvae. *RT-PCR analysis revealed no differential expression of cat, gpx1a, nfe2l2a and casp3a in the eye of zebrafish larvae treated for 4 and 24 h with atRAL compared to DMSO control group. n≥48 larval eyes/group from n≥2 biological replicates. Statistical analysis carried out by one-way ANOVA followed by Dunnett's multiple comparison test. Data normalized to β-actin expression and 0.05% DMSO solution-treated group.*

4.4.2 Efficacy study of nanoformulated NGF as preventive treatment

The efficacy of nanoformulated NGF was assessed as preventive treatment against the visual impairment induced by atRAL. IVT injections of free or nanoformulated NGF were performed 16 h prior to the exposure to 15 µM atRAL, and the visual acuity was assessed by OKR after 24 h. The number of saccades recorded in the 0.05% DMSO vehicle control (26 ± 2.28 saccades per minute) was significantly higher (**, p=0.0027) compared to the atRAL-treated group (15.08 ± 2.59 saccades per minute). The preventive injection of free NGF (16.38 ± 1.75 saccades per minute) or ANP:PNA-conjugated NGF (17.85 ± 1.47 saccades per minute) was not able to rescue visual function impaired by the exposure to atRAL, thus resulting in a significant reduction of the number of saccades (**, p=0.01 and *, p=0.04, respectively) compared to the negative control group. Besides, no differences were observed between free and nanoformulated NGF-pre-treated larvae and DPBS-injected controls exposed to atRAL (ns, p>0.05) (**Figure 27**).

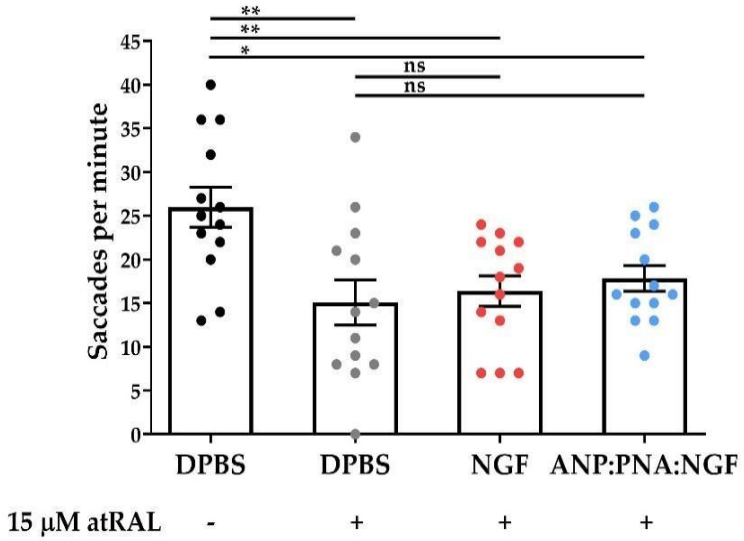

Figure 27. Intravitreal injection of ANP:PNA-conjugated NGF did not rescue all-trans retinal (atRAL)-induced visual impairment in zebrafish larvae. *Evaluation of visual function by OKR assay in zebrafish larvae pre-treated with free or nanoformulated NGF and exposed to atRAL. Negative control group was IVT injected with DPBS and treated with 0.05% DMSO solution. n=13 larvae/group from one biological replicate. Data analysed by one-way ANOVA followed by Tukey's multiple comparisons test. ns, p>0.05; *, p<0.05; **, p<0.01.*

5. DISCUSSION

5.1 Polymeric multi-functional nanoparticles: a promising ocular drug delivery system against oxidative stress in the retina

This Ph.D. project aimed to develop a smart nano-based drug delivery system as a preventive strategy against retinal degeneration or dysfunction. Retinal degeneration is the leading cause of partial or total blindness and represent a shared hallmark of diseases affecting the posterior segment of the eye, including AMD, glaucoma, DR, as well as inherited retinal diseases [6]. Visual impairment stands as a critical health problem worldwide, leading to loss of independence and negatively affecting quality of life of patients. The treatment of diseases at the posterior segment of the eye is hampered by the presence of several ocular barriers, which preserve eye functionality and homeostasis and protect the organ from insults, but also limit the access to the retina [1].

The advancement of nanotechnology-based systems in ophthalmology is one of the most pursued approaches for implementing therapeutic strategies to counteract or delay vision loss using implants or drug delivery systems. Indeed, physic-chemical properties of materials at the nanoscale translate into the ability to overcome the ocular barriers and improve solubility, stability, and controllability of drugs, thus increasing the therapeutic efficiency and limiting the side effects associated with inappropriate administration routes, massive doses, and unfavourable kinetics of drugs [99]. These advantages are crucial to achieve therapeutical effect at this tissue district, thus making nano-based formulation superior compared to conventional administration of drugs.

As a matter of fact, FDA-approved nanosystem for ocular treatment are already available in the market. However, they are mainly addressed to the treatment of the anterior segment of the eye, including dry eye disease, uveitis, acute keratitis, and bacterial conjunctivitis, and they are administered topically [69]. Unfortunately, only less than 5% of the applied drug reaches the ocular posterior segment, as consequence topical instillation is not the optimal route for delivering drugs at the retina [42]. The gold standard for the treatment of ocular posterior segment is the intravitreal route, but it requires several injections to sustain drugs in the optimal therapeutic dose over time, thus leading to high costs, risk of infection and pain [5].

The development of nanocarriers able to improve drug profile and ensure a sustained drug release perfectly meets the need to reduce multiple injections, thus avoiding side effects. Particularly, polymers are incredibly employed as materials for drug delivery systems because

of their noticeable biodegradability, peculiar stimuli-responsiveness, mucosal adhesive properties, and biocompatibility [100,101].

During my Ph.D. project, we developed a multifunctional polyacrylamide-based ocular drug delivery system, and we assessed its neuroprotective effect against visual dysfunction *in vivo*, using a zebrafish model of retinal degeneration induced by oxidative stress, as previously developed by our group [90]. Indeed, oxidative stress in the retina is caused by both endogenous (high metabolic rate, aging) and exogenous (smoking, light exposure) stimuli, and its pathological involvement culminates in retinal degeneration, thus representing a key risk factor for ocular degenerative diseases [31,32]. To create an oxidative condition in the retina, zebrafish have been selected as model organism due to high genome homology and the same retinal stratification of different cell types shared with humans [84]. Moreover, their rapid development, which provides established visual function only at 3 days post-fertilization, in addition to the transparency of larvae, allowed to validate the efficacy of our smart nanocarrier *in vivo* by performing visual behavioural assessment and short-term studies in the early stages of development [88,102].

After the optimisation of the protocol used for carrying out the synthesis of polyacrylamide nanoparticles (ANPs), we produced a fluorescent nanocarrier containing Alexa Fluor 488 dye for obtaining a polymeric nanosystem easily traceable in transparent zebrafish larvae for *in vivo* imaging to study the localisation of the particles after IVT injections in larvae at 3 days post-fertilization. We observed that our polymeric nanoparticles spontaneously migrate through the retinal layers over time, as suggested by their presence mainly at the level of the ganglion cell layer after 4 hpi and their autonomous distribution towards photoreceptor and retinal pigment epithelium layers after 24 hpi (**Figure 8**). Importantly, no particles were found to diffuse in the contralateral uninjected eye (**Figure 9**). Unfortunately, *in vivo* imaging highlighted the presence of nanoparticles at the level of the pronephros, the ancestral kidney of vertebrate embryos, where they started accumulating already at 4 hpi (**Figure 10**). Due to their instability in the eye, we moved forward an improvement of the nanocarrier formulation by exploiting the easiness of the polyacrylamide nanoparticles to be functionalised, taking advantage of the presence of several functional groups on their surface. Therefore, we selected PNA for stabilizing our polymeric nanocarrier in the ocular environment and conferring an active targeting capacity, thus improving its applicability as an ocular drug delivery system. Indeed, PNA is known to specifically bind cone photoreceptors due to the high affinity for their galactose-galactosamine disaccharide residues, as demonstrated also in humans and fish [103].

After the characterisation of the red fluorescent ANP:PNA, revealing an increase in the hydrodynamic diameter compared to the naked formulation (**Figure 7**) and good conjugation

properties, *in vivo* studies showed a promising modification in the biodistribution of our nanocarrier. The presence of the fluorescent dye Alexa Fluor 594 contained in the polyacrylamide matrix as well as of a FITC fluorophore conjugated to the PNA, easily allowed us to simultaneously follow the destiny of our nanocarrier and its cargo, respectively. After the IVT injection in 3 dpf larvae, the PNA-conjugated polymeric nanoparticles stably localised in the injected eye over time, without spreading in the contralateral eye and in any other larval tissues (**Figure 11**). On the contrary, naked ANPs were found in the pronephros at 24 hpi, thus suggesting their migration from the eye (**Figure 11**). The strong improvement in the localisation profile of the PNA-conjugated ANPs strongly suggests the ability of the lectin to prolong the residence time of the polymeric nanocarrier and its stability.

To implement a drug delivery system as a smart neuroprotective strategy targeting the posterior segment of the eye, we further functionalised the polyacrylamide nanoparticle surface using the NGF as a neuroprotectant against retinal degeneration. Indeed, several studies demonstrated that the NGF exerts pro-survival and regenerative effects in pre-clinical and clinical models of glaucoma [60-62], DR [63], and AMD [64] through the activation of different molecular pathways. Although there is a robust body of evidence reporting the beneficial effect of the neurotrophin against retinal degeneration, NGF-based therapies are at the very early stages of market approval and clinical applicability due to several drawbacks that still require a solution, such as poor solubility, low delivery efficiency, short half-life, and off-target effect [67]. To overcome these limitations, our group previously implemented an inorganic nanoformulation carrying the NGF. Our previous results demonstrated increased stability and protection from degradation, resulting in increased prevention of retinal ganglion cell loss, upon conjugation of NGF with magnetic nanoparticles [90]. Although these NGF-functionalised magnetic nanoparticles emerged as a promising ocular-tailored therapeutical nanotool, we decided to move towards an organic drug delivery system to overcome some disadvantages associated with the lack of evidence concerning biodegradability, toxicity and clearance mechanisms, which still pose some issues to the use of iron-based nanomaterials for the treatment of retinal disorders.

Hence, our PNA-targeted polyacrylamide-based nanocarrier has been further functionalised with NGF via a non-covalent reaction, revealing a shift in the hydrodynamic diameter (**Figure 7**), and a high conjugation efficiency. The bioactivity assessment of the nanoformulated NGF demonstrated its unaltered capacity in promoting the differentiation of PC12 cells in a neuron-like phenotype compared to the free factor, thus suggesting that the conjugated NGF was biologically active (**Figure 12**). Further, to test the neuroprotective effect of our nanocarrier, we induced a condition of oxidative stress in human RPE cells by co-incubating hydrogen peroxide with free or ANP:PNA-conjugated NGF. In sharp contrast with evidence reported in

the literature [104], we found that only the ANP:PNA-nanoformulated NGF, but not the free form, was able to exert a protective effect against the H_2O_2-elicited oxidative damage, as indicated by the higher percentage of metabolically-active cells in the ANP:PNA:NGF co-treated group (**Figure 14**). This difference can be attributed to the modality of cell treatment. Indeed, Cao *et al.* performed a pre-treatment with NGF before the exposure to oxidative stress, while we carried out a co-treatment with free or ANP:PNA-conjugated neurotrophin and hydrogen peroxide. Our result thus allows to speculate about an increased stability of NGF in an oxidative condition only when nanoformulated, which translates in a protective effect.

To corroborate these encouraging results regarding the biological activity of the nanoformulation, we decided to validate the neuroprotective ability of ANP:PNA-conjugated NGF *in vivo* using an ocular model of oxidative stress in zebrafish, previously developed by our group. As expected, the visual behavioural assessment carried out through the OKR assay revealed an impaired vision of larvae IVT injected with hydrogen peroxide compared to the saline-injected group. Most importantly, only the larvae pre-treated with ANP:PNA-conjugated NGF showed a number of saccades significantly higher compared to positive control larvae as well as the free NGF- and ANP:NGF-pre-treated group (**Figure 15**). Conversely, neither the preventive intraocular injection of the free NGF nor ANP:NGF was able to improve the visual function impaired by the induction of oxidative injury (**Figure 15**). These results are in line with our previous findings demonstrating an improved neuroprotection capability of NGF loaded in a drug delivery system compared to the free neurotrophin, thus suggesting a potential increase of its stability. In addition, the difference between the two NGF-based nanoformulations guide us to speculate on increased bioavailability of the NGF in the eye only when combined with PNA, thus resulting in a significant improvement of visual function.

In line with the data collected from the behavioural analysis, we also found a strong increase in the number of apoptotic cells in the retina of larvae IVT injected with H_2O_2 compared to the negative control group. These results were obtained through the analysis of apoptosis by both TUNEL and immunostaining against active caspase 3 assays and are in line with evidence reported in the literature according to which the apoptotic event is strictly related to retinal degeneration as consequence of oxidative stress [90,97]. Most encouraging, the preventive treatment with ANP:PNA-conjugated NGF, but not the injection of the free neurotrophin, resulted in a statistically significant reduction of both TUNEL- and active caspase 3-positive cells in the retina of injected larvae compared to the positive control (**Figures 16** and **17**), thus suggesting the ability of our ANP:PNA-formulated NGF in preventing oxidative stress-triggered apoptosis.

5.2 Cigarette smoke extract and all-*trans* retinal exposures: pharmacological modulations for the comprehension of visual impairment

The present Ph.D. project also investigated the effect of exogenous administration of cigarette smoke extract (CSE) and all-*trans* retinal (atRAL), a highly reactive metabolite produced during the visual cycle [98], in zebrafish larvae as potential new pharmacological approaches for modelling retinal degeneration, with the aim to deeper understanding of the molecular mechanisms that affect visual function and to assess the efficacy of therapeutics.
Indeed, both smoking and constant/prolonged light exposure are widely recognised as risk factors associated with the pathogenesis of retinal degenerative diseases through mechanisms of oxidative stress [105,106]. Particularly, zebrafish larvae were exposed to atRAL and CSE, and both visual behaviour and transcriptomic profile of oxidative stress biomarkers were studied by evaluating optokinetic and visual motor responses and RT-PCR, respectively. After the characterization of the two models of impaired visual function, we performed experiments aimed to evaluate the neuroprotective activity of NGF-based nanoformulation, previously developed during my research activities.

Cigarette smoking is an environmental pathological factor for cancer, cardiovascular and respiratory diseases, but it is also considered as the only modifiable risk factor for AMD. CSE is an oxidant mixture of more than 4000 genotoxic and carcinogenic compounds, which enhances the production of free radicals and contributes to AMD pathophysiology [107]. Evidence collected on human RPE cells demonstrated that CSE leads to oxidative stress, inflammatory processes, apoptosis, complement activation, endoplasmic reticulum stress and lipid dysregulation [108,109]. A few mice studies reported the contribution of CSE in causing choroidal neovascularization and sub-retinal deposits [110-112]. Moreover, previous studies using zebrafish for investigating the effect of cigarette smoke condensate focused on developmental and cardiac toxicity at the early development (<96 hours post-fertilization), thus mainly evaluating its broad harmful effect on general physiology and not considering the impact of CSE on visual behaviour [113,114].
Here, we demonstrated for the first time that the exposure of zebrafish larvae to CSE for 24 h negatively affected visual function. Indeed, as supported by carrying out different behavioural assays, both visual acuity and locomotor activity in response to light changes displayed a significant reduction in CSE-treated larvae compared to controls (**Figures 18**, **19** and **20**), thus contributing to extend the study of the impact of CSE on vision instead of broad systemic

alterations. Moreover, for elucidating any potential underlying molecular mechanisms, which specifically occurred in the eye as a consequence of CSE exposure, we analysed the relative expression of *cat*, *gpx1a*, *nfe2l2a* and *casp3a* as genes encoding for factors involved in the response against oxidative stress. No differences emerged in the relative expression of *cat*, *nfe2l2a* and *casp3a* after 4 and 24 h of CSE exposure (**Figure 21**). Despite studies reported in literature demonstrated an increase in *nfe2l2a* mRNA level after CSE treatment, they were carried out in *in vitro* models, and no evidence emerged from other investigations *in vivo*. However, the relative expression of *gpx1a* mRNA resulted significantly higher in the eye of CSE-treated larvae both after 4 and 24 h of acute exposure compared to the controls (**Figure 21**), thus suggesting the potential contribution of glutathione peroxidase-1 as a detoxifying enzyme acting in the molecular response against the oxidative stress triggered by CSE exposure. This data is also in line with previous studies in *Gpx1*-/- mice, reporting an increased susceptibility to the oxidative stress-inducing agents, including CSE [115,116]. Moreover, Timme-Laragy *et al.* demonstrated that the mRNA levels of several antioxidant enzymes, including *gpx1a*, increased in zebrafish larvae exposed to polycyclic aromatic hydrocarbons, which are components of cigarette smoke [117]. Basing on these new evidence and knowing the protective effect of our ANP:PNA-conjugated NGF against oxidative stress, we used this novel zebrafish model of CSE-induced visual impairment for further assessing the efficacy of our smart nanoformulation.

Prior administration of NGF-based nanoformulation into the eye of zebrafish larvae showed a promising neuroprotective effect against the reduction of visual function induced by CSE treatment. Although no statistically significant difference emerged between ANP:PNA:NGF-injected larvae and the CSE-treated ones in the visual motor response (**Figure 23**), a promising trend of improved locomotor activity was observed. Most importantly, we demonstrated that our NGF-based nanoformulation was able to improve the optokinetic response of zebrafish larvae compromised by acute systemic treatment with CSE (**Figure 22**), and the similar result obtained by using free NGF and its polymeric nanoformulation was not unexpected due to the acute experimental time frame. Thus, taking advantage from a zebrafish model of pharmacological modulation of visual behaviour, we were able to further assess the neuroprotective efficacy of our nanocarrier, paving the way for the development of neurotrophin-based therapeutical strategies against CSE-induced retinal degeneration. Notably, this is the first study demonstrating neurotrophin NGF rescue of visual function in zebrafish larvae negatively affected by systemic exposure to CSE.

All-*trans* retinal is a reactive aldehyde endogenously produced during the visual cycle as a consequence of photon detection by the photosensitive pigment (opsin) in outer segments of

photoreceptors. Indeed, light absorption leads to convert the 11-cis-retinal, a chromophore covalently bound to the opsin, in all-*trans* retinal, which is then release from opsin, reduced to all-*trans* retinol and transported to the retinal pigment epithelium. There, it is further recycled to 11-cis-retinal before to be shuttled back to the photoreceptor for regenerating opsin and complete the visual cycle [98]. atRAL is a potent photosensitizer and alterations in its clearance, so its accumulation in photoreceptors and RPE, is associated with retinal photodamage and pathogenesis of AMD. Indeed, numerous *in vitro* and *in vivo* research reported that the accumulation of atRAL plays a detrimental role in retinal degeneration through ROS overproduction, which in turn causes autophagic cell death, ferroptosis, ER stress and mitochondrial dysfunction [118,119].

Here, we wanted to deepen how the exposure to atRAL impact on vision. Zebrafish larvae showed a strong reduction of optokinetic response after 24 h of atRAL treatment compared to controls (**Figure 24**), thus suggesting that an excess of atRAL exogenously administered negatively affected visual function. No studies in the literature reported a decrease of visual function *in vivo* as a consequence of atRAL accumulation. Using a simple but powerful system for evaluating the effect of compounds on vision, such as OKR, we were able to confirm that exogenous administration of atRAL exert oculotoxicity. Thus, to further investigate the contribution of atRAL on visual behaviour, we also analysed the visual motor response. Despite no alteration in the visual motor response emerged (**Figure 25**), further studies aiming to improve the assay design might be worthwhile to obtain a VMR phenotype. Indeed, although the VMR was assessed basing on an optimised protocol published in the literature [95], the length of each light onset and offset periods could be extended in order to enhance the light adaptation of the larvae and maximize the response to light changes. To preliminary investigate any potential molecular mechanism underlaying the impairment of visual function induced by atRAL, differential gene expression of oxidative stress biomarkers was analysed. Although studies in ARPE-19 cells showed that the accumulation of atRAL induced an up-regulation of Nrf2 mRNA level due to ROS overproduction, as well as a caspase-dependent apoptosis of RPE cells after 6 h of treatment [120], no significant differences in the relative expression of *nfe2l2a* and *casp3a* were observed in atRAL-treated larvae compared to the controls (**Figure 26**). Moreover, the transcriptomic profile of oxidative stress biomarkers, such as *cat* and *gpx1a*, did not show a differential profile between atRAL-treated and control groups (**Figure 26**), probably due to the non-optimal time points selected for analysing a variation in the gene expression. Despite no upregulation of antioxidant enzymes emerged, we decided to evaluate our smart NGF-based nanocarriers as protective treatment against atRAL being known the role of neurotrophins in promoting photoreceptor and RPE cell survival [121]. Additionally, a recent study carried out by Cocchiaro and collaborators demonstrated

that the IVT injection of recombinant human NGF in adult zebrafish after 60 h of exposure to light irradiation leads to the upregulation of the ERK1/2 pathway, inducing photoreceptor regeneration promoted by Müller glia cells and a consequent increase of the outer nuclear layer thickness [122].

Prior ocular administration of NGF-based nanoformulation in atRAL-treated zebrafish larvae did not result in an improved optokinetic response (**Figure 27**). This could be attributed to a deficient protective mechanism able to counteract the retinal dysfunction induced by the atRAL. Indeed, the negative impact of atRAL on visual behaviour resulted more severe than the one triggered by CSE exposure, as shown by a more drastic reduction in the optokinetic response of atRAL-treated larvae, thus leading to an ocular impairment more difficult to rescue. Although the rhNGF-triggered retinal regeneration published by Cocchiaro *et al.* demonstrated a great potential in recovering retinal tissue after injury, no evidence of functional photoreceptors have been collected. Moreover, in contrast to fish and amphibians, in which retinal regeneration is strongly supported by the presence of proliferating neural progenitors at the ciliary marginal zone (CMZ) [123], regenerative process in human retina is hindered by both the absence of CMZ and the limited research supporting the response of Müller glial cells in restoration of visual function in humans [124].

Further experiments are thus needed to enhance the efficacy of nanoformulated NGF as a neuroprotective strategy as well as to better elucidate molecular pathway underlying the visual impairment observed in zebrafish in response to atRAL accumulation, hence helping in the comprehension of promising paths for the development of therapeutical treatments.

5.3 Future perspectives

This study aimed to develop smart nanoparticles able to target the posterior segment of the eye and exert a neuroprotective effect against retinal dysfunction triggered by oxidative stress. Our multifunctional NGF-based nanoformulation showed encouraging evidence related to the ability of the nanocarrier in improving the residence time and the bioavailability of NGF at the targeted site, thus resulting in enhanced optokinetic response and reduced level of apoptosis in the retina exposed to oxidative stress. However, further experiments are needed to investigate how long our nanocarrier can protect NGF and ensure its sustained neuroprotective release. Moreover, a deeper toxicological assessment is required to investigate any potential toxic effect caused by the prolonged retention of polyacrylamide nanoparticles in the ocular environment as well as to assess their biodegradability and elimination mechanisms. Future perspective aims to extend the study to rodent models to gain new evidence about safety and efficacy profiles of our nanoformulation.

5.4 Limitation of the study

Here, we developed smart neuroprotective nanoparticles as a promising ocular drug delivery system to be implemented for preventing retinal degeneration. The bioactivity of the nanoformulation has been validated *in vitro* and its neuroprotective efficacy has been deeply investigated *in vitro* on human retinal pigment epithelial cells as well as *in vivo* using zebrafish models of oxidative stress, showing the ability to protect the retina from the oxidative damage at both behavioural and functional level. Although the collected results allowed us to speculate about enhanced drug stability and bioavailability as well as targeting specificity of our smart nanocarrier, no evaluations have been performed to prove that nanoparticles do not cross the blood-brain barrier, whose structural features are comparable to the blood-retinal barrier, thus avoiding any potential deleterious effect. Moreover, despite no ocular toxicity emerged from the IVT injection of our polymeric nanocarriers over time, no studies have been carried out to evaluate the clearance of the nanocarriers after injection for a better understanding of its degradation and elimination profiles. Lastly, a deeper morphological characterization of the nanoformulation, i.e., by TEM analysis, as well as data related to the consistency of functionalisation and its stability are missing. As shape, size distribution of the particles and surface charge can influence toxicity and biodistribution of a nanocarrier, they represent crucial aspects to be assessed.

REFERENCES

1. Kaplan, H.J. Anatomy and function of the eye. *Chem Immunol Allergy* **2007**, *92*, 4-10, doi:10.1159/000099236.
2. Salesse, C. [Physiology of the visual retinal signal: From phototransduction to the visual cycle]. *J Fr Ophtalmol* **2017**, *40*, 239-250, doi:10.1016/j.jfo.2016.12.006.
3. Grigoryan, E.N. Self-Organization of the Retina during Eye Development, Retinal Regeneration In Vivo, and in Retinal 3D Organoids In Vitro. *Biomedicines* **2022**, *10*, doi:10.3390/biomedicines10061458.
4. Tsai, C.H.; Wang, P.Y.; Lin, I.C.; Huang, H.; Liu, G.S.; Tseng, C.L. Ocular Drug Delivery: Role of Degradable Polymeric Nanocarriers for Ophthalmic Application. *Int J Mol Sci* **2018**, *19*, doi:10.3390/ijms19092830.
5. Karamali, F.; Behtaj, S.; Babaei-Abraki, S.; Hadady, H.; Atefi, A.; Savoj, S.; Soroushzadeh, S.; Najafian, S.; Nasr Esfahani, M.H.; Klassen, H. Potential therapeutic strategies for photoreceptor degeneration: the path to restore vision. *J Transl Med* **2022**, *20*, 572, doi:10.1186/s12967-022-03738-4.
6. World Health Organization. Available online: https://www.who.int/news-room/fact-sheets/detail/blindness-and-visual-impairment#:~:text=Globally%2C%20at%20least%202.2%20billion,has%20yet%20to%20be%20addressed.
7. Tham, Y.C.; Li, X.; Wong, T.Y.; Quigley, H.A.; Aung, T.; Cheng, C.Y. Global prevalence of glaucoma and projections of glaucoma burden through 2040: a systematic review and meta-analysis. *Ophthalmology* **2014**, *121*, 2081-2090, doi:10.1016/j.ophtha.2014.05.013.
8. Weinreb, R.N.; Aung, T.; Medeiros, F.A. The pathophysiology and treatment of glaucoma: a review. *JAMA* **2014**, *311*, 1901-1911, doi:10.1001/jama.2014.3192.
9. Allison, K.; Patel, D.; Alabi, O. Epidemiology of Glaucoma: The Past, Present, and Predictions for the Future. *Cureus* **2020**, *12*, e11686, doi:10.7759/cureus.11686.
10. Schuster, A.K.; Erb, C.; Hoffmann, E.M.; Dietlein, T.; Pfeiffer, N. The Diagnosis and Treatment of Glaucoma. *Dtsch Arztebl Int* **2020**, *117*, 225-234, doi:10.3238/arztebl.2020.0225.
11. Wong, W.L.; Su, X.; Li, X.; Cheung, C.M.; Klein, R.; Cheng, C.Y.; Wong, T.Y. Global prevalence of age-related macular degeneration and disease burden projection for 2020 and 2040: a systematic review and meta-analysis. *Lancet Glob Health* **2014**, *2*, e106-116, doi:10.1016/S2214-109X(13)70145-1.

12. Mitchell, P.; Liew, G.; Gopinath, B.; Wong, T.Y. Age-related macular degeneration. *Lancet* **2018**, *392*, 1147-1159, doi:10.1016/S0140-6736(18)31550-2.
13. Gehrs, K.M.; Anderson, D.H.; Johnson, L.V.; Hageman, G.S. Age-related macular degeneration--emerging pathogenetic and therapeutic concepts. *Ann Med* **2006**, *38*, 450-471, doi:10.1080/07853890600946724.
14. Thomas, C.J.; Mirza, R.G.; Gill, M.K. Age-Related Macular Degeneration. *Med Clin North Am* **2021**, *105*, 473-491, doi:10.1016/j.mcna.2021.01.003.
15. Lightman, S.; Towler, H.M. Diabetic retinopathy. *Clin Cornerstone* **2003**, *5*, 12-21, doi:10.1016/s1098-3597(03)90015-9.
16. Teo, Z.L.; Tham, Y.C.; Yu, M.; Chee, M.L.; Rim, T.H.; Cheung, N.; Bikbov, M.M.; Wang, Y.X.; Tang, Y.; Lu, Y.; et al. Global Prevalence of Diabetic Retinopathy and Projection of Burden through 2045: Systematic Review and Meta-analysis. *Ophthalmology* **2021**, *128*, 1580-1591, doi:10.1016/j.ophtha.2021.04.027.
17. Lin, K.Y.; Hsih, W.H.; Lin, Y.B.; Wen, C.Y.; Chang, T.J. Update in the epidemiology, risk factors, screening, and treatment of diabetic retinopathy. *J Diabetes Investig* **2021**, *12*, 1322-1325, doi:10.1111/jdi.13480.
18. Hurley, J.B.; Lindsay, K.J.; Du, J. Glucose, lactate, and shuttling of metabolites in vertebrate retinas. *J Neurosci Res* **2015**, *93*, 1079-1092, doi:10.1002/jnr.23583.
19. Harris, J.J.; Jolivet, R.; Attwell, D. Synaptic energy use and supply. *Neuron* **2012**, *75*, 762-777, doi:10.1016/j.neuron.2012.08.019.
20. Pham-Huy, L.A.; He, H.; Pham-Huy, C. Free radicals, antioxidants in disease and health. *Int J Biomed Sci* **2008**, *4*, 89-96.
21. Álvarez-Barrios, A.; Álvarez, L.; García, M.; Artime, E.; Pereiro, R.; González-Iglesias, H. Antioxidant Defenses in the Human Eye: A Focus on Metallothioneins. *Antioxidants (Basel)* **2021**, *10*, doi:10.3390/antiox10010089.
22. Batliwala, S.; Xavier, C.; Liu, Y.; Wu, H.; Pang, I.H. Involvement of Nrf2 in Ocular Diseases. *Oxid Med Cell Longev* **2017**, *2017*, 1703810, doi:10.1155/2017/1703810.
23. Mittal, M.; Siddiqui, M.R.; Tran, K.; Reddy, S.P.; Malik, A.B. Reactive oxygen species in inflammation and tissue injury. *Antioxid Redox Signal* **2014**, *20*, 1126-1167, doi:10.1089/ars.2012.5149.
24. De Gaetano, A.; Gibellini, L.; Zanini, G.; Nasi, M.; Cossarizza, A.; Pinti, M. Mitophagy and Oxidative Stress: The Role of Aging. *Antioxidants (Basel)* **2021**, *10*, doi:10.3390/antiox10050794.
25. Chang, K.C.; Liu, P.F.; Chang, C.H.; Lin, Y.C.; Chen, Y.J.; Shu, C.W. The interplay of autophagy and oxidative stress in the pathogenesis and therapy of retinal degenerative diseases. *Cell Biosci* **2022**, *12*, 1, doi:10.1186/s13578-021-00736-9.

26. Chrysostomou, V.; Rezania, F.; Trounce, I.A.; Crowston, J.G. Oxidative stress and mitochondrial dysfunction in glaucoma. *Curr Opin Pharmacol* **2013**, *13*, 12-15, doi:10.1016/j.coph.2012.09.008.
27. Dammak, A.; Huete-Toral, F.; Carpena-Torres, C.; Martin-Gil, A.; Pastrana, C.; Carracedo, G. From Oxidative Stress to Inflammation in the Posterior Ocular Diseases: Diagnosis and Treatment. *Pharmaceutics* **2021**, *13*, doi:10.3390/pharmaceutics13091376.
28. Nita, M.; Grzybowski, A. The Role of the Reactive Oxygen Species and Oxidative Stress in the Pathomechanism of the Age-Related Ocular Diseases and Other Pathologies of the Anterior and Posterior Eye Segments in Adults. *Oxid Med Cell Longev* **2016**, *2016*, 3164734, doi:10.1155/2016/3164734.
29. Li, G.Y.; Osborne, N.N. Oxidative-induced apoptosis to an immortalized ganglion cell line is caspase independent but involves the activation of poly(ADP-ribose)polymerase and apoptosis-inducing factor. *Brain Res* **2008**, *1188*, 35-43, doi:10.1016/j.brainres.2007.10.073.
30. Li, B.; Ning, B.; Yang, F.; Guo, C. Nerve Growth Factor Promotes Retinal Neurovascular Unit Repair: A Review. *Curr Eye Res* **2022**, *47*, 1095-1105, doi:10.1080/02713683.2022.2055084.
31. Ozawa, Y. Oxidative stress in the light-exposed retina and its implication in age-related macular degeneration. *Redox Biol* **2020**, *37*, 101779, doi:10.1016/j.redox.2020.101779.
32. Kumar, D.M.; Agarwal, N. Oxidative stress in glaucoma: a burden of evidence. *J Glaucoma* **2007**, *16*, 334-343, doi:10.1097/01.ijg.0000243480.67532.1b.
33. Tezel, G. Oxidative stress in glaucomatous neurodegeneration: mechanisms and consequences. *Prog Retin Eye Res* **2006**, *25*, 490-513, doi:10.1016/j.preteyeres.2006.07.003.
34. Yanagi, M.; Kawasaki, R.; Wang, J.J.; Wong, T.Y.; Crowston, J.; Kiuchi, Y. Vascular risk factors in glaucoma: a review. *Clin Exp Ophthalmol* **2011**, *39*, 252-258, doi:10.1111/j.1442-9071.2010.02455.x.
35. O'Hare Doig, R.L.; Bartlett, C.A.; Maghzal, G.J.; Lam, M.; Archer, M.; Stocker, R.; Fitzgerald, M. Reactive species and oxidative stress in optic nerve vulnerable to secondary degeneration. *Exp Neurol* **2014**, *261*, 136-146, doi:10.1016/j.expneurol.2014.06.007.
36. Somasundaran, S.; Constable, I.J.; Mellough, C.B.; Carvalho, L.S. Retinal pigment epithelium and age-related macular degeneration: A review of major disease mechanisms. *Clin Exp Ophthalmol* **2020**, *48*, 1043-1056, doi:10.1111/ceo.13834.
37. Tong, Y.; Zhang, Z.; Wang, S. Role of Mitochondria in Retinal Pigment Epithelial Aging and Degeneration. *Front Aging* **2022**, *3*, 926627, doi:10.3389/fragi.2022.926627.

38. Wong, T.Y.; Cheung, C.M.; Larsen, M.; Sharma, S.; Simó, R. Diabetic retinopathy. *Nat Rev Dis Primers* **2016**, *2*, 16012, doi:10.1038/nrdp.2016.12.
39. Wang, Z.; Zhao, H.; Guan, W.; Kang, X.; Tai, X.; Shen, Y. Metabolic memory in mitochondrial oxidative damage triggers diabetic retinopathy. *BMC Ophthalmol* **2018**, *18*, 258, doi:10.1186/s12886-018-0921-0.
40. Cervellati, F.; Cervellati, C.; Romani, A.; Cremonini, E.; Sticozzi, C.; Belmonte, G.; Pessina, F.; Valacchi, G. Hypoxia induces cell damage via oxidative stress in retinal epithelial cells. *Free Radic Res* **2014**, *48*, 303-312, doi:10.3109/10715762.2013.867484.
41. Mannermaa, E.; Vellonen, K.S.; Urtti, A. Drug transport in corneal epithelium and blood-retina barrier: emerging role of transporters in ocular pharmacokinetics. *Adv Drug Deliv Rev* **2006**, *58*, 1136-1163, doi:10.1016/j.addr.2006.07.024.
42. Awwad, S.; Mohamed Ahmed, A.H.A.; Sharma, G.; Heng, J.S.; Khaw, P.T.; Brocchini, S.; Lockwood, A. Principles of pharmacology in the eye. *Br J Pharmacol* **2017**, *174*, 4205-4223, doi:10.1111/bph.14024.
43. Liu, Y.; Chen, S.J.; Li, S.Y.; Qu, L.H.; Meng, X.H.; Wang, Y.; Xu, H.W.; Liang, Z.Q.; Yin, Z.Q. Long-term safety of human retinal progenitor cell transplantation in retinitis pigmentosa patients. *Stem Cell Res Ther* **2017**, *8*, 209, doi:10.1186/s13287-017-0661-8.
44. Ikelle, L.; Al-Ubaidi, M.R.; Naash, M.I. Pluripotent Stem Cells for the Treatment of Retinal Degeneration: Current Strategies and Future Directions. *Front Cell Dev Biol* **2020**, *8*, 743, doi:10.3389/fcell.2020.00743.
45. Hinkle, J.W.; Mahmoudzadeh, R.; Kuriyan, A.E. Cell-based therapies for retinal diseases: a review of clinical trials and direct to consumer "cell therapy" clinics. *Stem Cell Res Ther* **2021**, *12*, 538, doi:10.1186/s13287-021-02546-9.
46. Maya-Vetencourt, J.F.; Manfredi, G.; Mete, M.; Colombo, E.; Bramini, M.; Di Marco, S.; Shmal, D.; Mantero, G.; Dipalo, M.; Rocchi, A.; et al. Subretinally injected semiconducting polymer nanoparticles rescue vision in a rat model of retinal dystrophy. *Nat Nanotechnol* **2020**, *15*, 698-708, doi:10.1038/s41565-020-0696-3.
47. Riley, M.K.; Vermerris, W. Recent Advances in Nanomaterials for Gene Delivery-A Review. *Nanomaterials (Basel)* **2017**, *7*, doi:10.3390/nano7050094.
48. FDA approves hereditary blindness gene therapy. *Nat Biotechnol* **2018**, *36*, 6, doi:10.1038/nbt0118-6a.
49. European Medicines Agency. Available online: https://www.ema.europa.eu/en/documents/overview/luxturna-epar-medicine-overview_en.pdf.

50. Bansal, M.; Acharya, S.; Sharma, S.; Phutela, R.; Rauthan, R.; Maiti, S.; Chakraborty, D. CRISPR Cas9 based genome editing in inherited retinal dystrophies. *Ophthalmic Genet* **2021**, *42*, 365-374, doi:10.1080/13816810.2021.1904421.
51. Adijanto, J.; Naash, M.I. Nanoparticle-based technologies for retinal gene therapy. *Eur J Pharm Biopharm* **2015**, *95*, 353-367, doi:10.1016/j.ejpb.2014.12.028.
52. Editas Medicine. Available online: https://ir.editasmedicine.com/news-releases/news-release-details/editas-medicine-announces-clinical-data-demonstrating-proof.
53. Maneu, V.; Lax, P.; Cuenca, N. Current and future therapeutic strategies for the treatment of retinal neurodegenerative diseases. *Neural Regen Res* **2022**, *17*, 103-104, doi:10.4103/1673-5374.314305.
54. Del Rio, P.; Hauck, S.M.; Irmler, M.; Tripathi, P.; Beckers, J.; Goetz, M.; Ueffing, M. Gene Expression Analysis of GDNF-induced Mueller Glial Cell-derived Neuroprotective Factors: Possible Candidates for Photoreceptor Survival. ***Invest. Ophthalmol. Vis. Sci.*** **2009**, 50(13):691.
55. Read, S.P.; Cashman, S.M.; Kumar-Singh, R. POD nanoparticles expressing GDNF provide structural and functional rescue of light-induced retinal degeneration in an adult mouse. *Mol Ther* **2010**, *18*, 1917-1926, doi:10.1038/mt.2010.167.
56. Zhang, K.; Hopkins, J.J.; Heier, J.S.; Birch, D.G.; Halperin, L.S.; Albini, T.A.; Brown, D.M.; Jaffe, G.J.; Tao, W.; Williams, G.A. Ciliary neurotrophic factor delivered by encapsulated cell intraocular implants for treatment of geographic atrophy in age-related macular degeneration. *Proc Natl Acad Sci U S A* **2011**, *108*, 6241-6245, doi:10.1073/pnas.1018987108.
57. Birch, D.G.; Weleber, R.G.; Duncan, J.L.; Jaffe, G.J.; Tao, W.; Groups, C.N.F.R.P.S. Randomized trial of ciliary neurotrophic factor delivered by encapsulated cell intraocular implants for retinitis pigmentosa. *Am J Ophthalmol* **2013**, *156*, 283-292.e281, doi:10.1016/j.ajo.2013.03.021.
58. Domenici, L.; Origlia, N.; Falsini, B.; Cerri, E.; Barloscio, D.; Fabiani, C.; Sansò, M.; Giovannini, L. Rescue of retinal function by BDNF in a mouse model of glaucoma. *PLoS One* **2014**, *9*, e115579, doi:10.1371/journal.pone.0115579.
59. Feng, L.; Chen, H.; Yi, J.; Troy, J.B.; Zhang, H.F.; Liu, X. Long-Term Protection of Retinal Ganglion Cells and Visual Function by Brain-Derived Neurotrophic Factor in Mice With Ocular Hypertension. *Invest Ophthalmol Vis Sci* **2016**, *57*, 3793-3802, doi:10.1167/iovs.16-19825.
60. Guo, L.; Davis, B.M.; Ravindran, N.; Galvao, J.; Kapoor, N.; Haamedi, N.; Shamsher, E.; Luong, V.; Fico, E.; Cordeiro, M.F. Topical recombinant human Nerve growth factor (rh-NGF) is

neuroprotective to retinal ganglion cells by targeting secondary degeneration. *Sci Rep* **2020**, *10*, 3375, doi:10.1038/s41598-020-60427-2.

61. Mesentier-Louro, L.A.; Rosso, P.; Carito, V.; Mendez-Otero, R.; Santiago, M.F.; Rama, P.; Lambiase, A.; Tirassa, P. Nerve Growth Factor Role on Retinal Ganglion Cell Survival and Axon Regrowth: Effects of Ocular Administration in Experimental Model of Optic Nerve Injury. *Mol Neurobiol* **2019**, *56*, 1056-1069, doi:10.1007/s12035-018-1154-1.
62. Beykin, G.; Stell, L.; Halim, M.S.; Nuñez, M.; Popova, L.; Nguyen, B.T.; Groth, S.L.; Dennis, A.; Li, Z.; Atkins, M.; et al. Phase 1b Randomized Controlled Study of Short Course Topical Recombinant Human Nerve Growth Factor (rhNGF) for Neuroenhancement in Glaucoma: Safety, Tolerability, and Efficacy Measure Outcomes. *Am J Ophthalmol* **2022**, *234*, 223-234, doi:10.1016/j.ajo.2021.11.002.
63. Zerbini, G.; Maestroni, S.; Leocani, L.; Mosca, A.; Godi, M.; Paleari, R.; Belvedere, A.; Gabellini, D.; Tirassa, P.; Castoldi, V.; et al. Topical nerve growth factor prevents neurodegenerative and vascular stages of diabetic retinopathy. *Front Pharmacol* **2022**, *13*, 1015522, doi:10.3389/fphar.2022.1015522.
64. Telegina, D.V.; Kolosova, N.G.; Kozhevnikova, O.S. Immunohistochemical localization of NGF, BDNF, and their receptors in a normal and AMD-like rat retina. *BMC Med Genomics* **2019**, *12*, 48, doi:10.1186/s12920-019-0493-8.
65. Falsini, B.; Iarossi, G.; Chiaretti, A.; Ruggiero, A.; Manni, L.; Galli-Resta, L.; Corbo, G.; Abed, E. NGF eye-drops topical administration in patients with retinitis pigmentosa, a pilot study. *J Transl Med* **2016**, *14*, 8, doi:10.1186/s12967-015-0750-3.
66. Rocco, M.L.; Calzà, L.; Aloe, L. NGF and Retinitis Pigmentosa: Structural and Molecular Studies. *Adv Exp Med Biol* **2021**, *1331*, 255-263, doi:10.1007/978-3-030-74046-7_17.
67. Alastra, G.; Aloe, L.; Baldassarro, V.A.; Calzà, L.; Cescatti, M.; Duskey, J.T.; Focarete, M.L.; Giacomini, D.; Giardino, L.; Giraldi, V.; et al. Nerve Growth Factor Biodelivery: A Limiting Step in Moving Toward Extensive Clinical Application? *Front Neurosci* **2021**, *15*, 695592, doi:10.3389/fnins.2021.695592.
68. Bayda, S.; Adeel, M.; Tuccinardi, T.; Cordani, M.; Rizzolio, F. The History of Nanoscience and Nanotechnology: From Chemical-Physical Applications to Nanomedicine. *Molecules* **2019**, *25*, doi:10.3390/molecules25010112.
69. Kagkelaris, K.; Panayiotakopoulos, G.; Georgakopoulos, C.D. Nanotechnology-based formulations to amplify intraocular bioavailability. *Ther Adv Ophthalmol* **2022**, *14*, 25158414221112356, doi:10.1177/25158414221112356.
70. Khiev, D.; Mohamed, Z.A.; Vichare, R.; Paulson, R.; Bhatia, S.; Mohapatra, S.; Lobo, G.P.; Valapala, M.; Kerur, N.; Passaglia, C.L.; et al. Emerging Nano-Formulations and

Nanomedicines Applications for Ocular Drug Delivery. *Nanomaterials (Basel)* **2021**, *11*, doi:10.3390/nano11010173.

71. Joudeh, N.; Linke, D. Nanoparticle classification, physicochemical properties, characterization, and applications: a comprehensive review for biologists. *J Nanobiotechnology* **2022**, *20*, 262, doi:10.1186/s12951-022-01477-8.
72. Zhang, J.; Jiao, J.; Niu, M.; Gao, X.; Zhang, G.; Yu, H.; Yang, X.; Liu, L. Ten Years of Knowledge of Nano-Carrier Based Drug Delivery Systems in Ophthalmology: Current Evidence, Challenges, and Future Prospective. *Int J Nanomedicine* **2021**, *16*, 6497-6530, doi:10.2147/IJN.S329831.
73. Subbiah, R.; Veerapandian, M.; Yun, K.S. Nanoparticles: functionalization and multifunctional applications in biomedical sciences. *Curr Med Chem* **2010**, *17*, 4559-4577, doi:10.2174/092986710794183024.
74. Zhou, H.Y.; Hao, J.L.; Wang, S.; Zheng, Y.; Zhang, W.S. Nanoparticles in the ocular drug delivery. *Int J Ophthalmol* **2013**, *6*, 390-396, doi:10.3980/j.issn.2222-3959.2013.03.25.
75. Zarbin, M.A.; Montemagno, C.; Leary, J.F.; Ritch, R. Nanomedicine in ophthalmology: the new frontier. *Am J Ophthalmol* **2010**, *150*, 144-162.e142, doi:10.1016/j.ajo.2010.03.019.
76. Hua, S.; de Matos, M.B.C.; Metselaar, J.M.; Storm, G. Current Trends and Challenges in the Clinical Translation of Nanoparticulate Nanomedicines: Pathways for Translational Development and Commercialization. *Front Pharmacol* **2018**, *9*, 790, doi:10.3389/fphar.2018.00790.
77. Afarid, M.; Mahmoodi, S.; Baghban, R. Recent achievements in nano-based technologies for ocular disease diagnosis and treatment, review and update. *J Nanobiotechnology* **2022**, *20*, 361, doi:10.1186/s12951-022-01567-7.
78. Li, K.; Zang, X.; Cheng, M.; Chen, X. Stimuli-responsive nanoparticles based on poly acrylic derivatives for tumor therapy. *Int J Pharm* **2021**, *601*, 120506, doi:10.1016/j.ijpharm.2021.120506.
79. Ding, Y.; Chow, S.H.; Chen, J.; Brun, A.P.L.; Wu, C.M.; Duff, A.P.; Wang, Y.; Song, J.; Wang, J.H.; Wong, V.H.Y.; et al. Targeted delivery of LM22A-4 by cubosomes protects retinal ganglion cells in an experimental glaucoma model. *Acta Biomater* **2021**, *126*, 433-444, doi:10.1016/j.actbio.2021.03.043.
80. Qiu, F.; Meng, T.; Chen, Q.; Zhou, K.; Shao, Y.; Matlock, G.; Ma, X.; Wu, W.; Du, Y.; Wang, X.; et al. Fenofibrate-Loaded Biodegradable Nanoparticles for the Treatment of Experimental Diabetic Retinopathy and Neovascular Age-Related Macular Degeneration. *Mol Pharm* **2019**, *16*, 1958-1970, doi:10.1021/acs.molpharmaceut.8b01319.
81. Maurice, D. The effect of the low blink rate in rabbits on topical drug penetration. *J Ocul Pharmacol Ther* **1995**, *11*, 297-304, doi:10.1089/jop.1995.11.297.

82. Chhetri, J.; Jacobson, G.; Gueven, N. Zebrafish--on the move towards ophthalmological research. *Eye (Lond)* **2014**, *28*, 367-380, doi:10.1038/eye.2014.19.
83. Bibliowicz, J.; Tittle, R.K.; Gross, J.M. Toward a better understanding of human eye disease insights from the zebrafish, Danio rerio. *Prog Mol Biol Transl Sci* **2011**, *100*, 287-330, doi:10.1016/B978-0-12-384878-9.00007-8.
84. Richardson, R.; Tracey-White, D.; Webster, A.; Moosajee, M. The zebrafish eye-a paradigm for investigating human ocular genetics. *Eye (Lond)* **2017**, *31*, 68-86, doi:10.1038/eye.2016.198.
85. Howe, K.; Clark, M.D.; Torroja, C.F.; Torrance, J.; Berthelot, C.; Muffato, M.; Collins, J.E.; Humphray, S.; McLaren, K.; Matthews, L.; et al. The zebrafish reference genome sequence and its relationship to the human genome. *Nature* **2013**, *496*, 498-503, doi:10.1038/nature12111.
86. Risner, M.L.; Lemerise, E.; Vukmanic, E.V.; Moore, A. Behavioral spectral sensitivity of the zebrafish (Danio rerio). *Vision Res* **2006**, *46*, 2625-2635, doi:10.1016/j.visres.2005.12.014.
87. Easter, S.S.; Nicola, G.N. The development of vision in the zebrafish (Danio rerio). *Dev Biol* **1996**, *180*, 646-663, doi:10.1006/dbio.1996.0335.
88. Haque, E.; Ward, A.C. Zebrafish as a Model to Evaluate Nanoparticle Toxicity. *Nanomaterials (Basel)* **2018**, *8*, doi:10.3390/nano8070561.
89. Pensado-López, A.; Fernández-Rey, J.; Reimunde, P.; Crecente-Campo, J.; Sánchez, L.; Torres Andón, F. Zebrafish Models for the Safety and Therapeutic Testing of Nanoparticles with a Focus on Macrophages. *Nanomaterials (Basel)* **2021**, *11*, doi:10.3390/nano11071784.
90. Giannaccini, M.; Usai, A.; Chiellini, F.; Guadagni, V.; Andreazzoli, M.; Ori, M.; Pasqualetti, M.; Dente, L.; Raffa, V. Neurotrophin-conjugated nanoparticles prevent retina damage induced by oxidative stress. *Cell Mol Life Sci* **2018**, *75*, 1255-1267, doi:10.1007/s00018-017-2691-x.
91. Rahimi, M.; Kilaru, S.; Sleiman, G.E.; Saleh, A.; Rudkevich, D.; Nguyen, K. Synthesis and Characterization of Thermo-Sensitive Nanoparticles for Drug Delivery Applications. *J Biomed Nanotechnol* **2008**, *4*, 482-490, doi:10.1166/jbn.2008.014.
92. Available online: https://zfin.org/.
93. Brockerhoff, S.E. Measuring the optokinetic response of zebrafish larvae. *Nat Protoc* **2006**, *1*, 2448-2451, doi:10.1038/nprot.2006.255.
94. Gómez Sánchez, A.; Álvarez, Y.; Colligris, B.; Kennedy, B.N. Affordable and effective optokinetic response methods to assess visual acuity and contrast sensitivity in larval to

juvenile zebrafish. Available online: https://open-research-europe.ec.europa.eu/articles/1-92 (accessed on 06 Jan 2022).

95. Deeti, S.; O'Farrell, S.; Kennedy, B.N. Early safety assessment of human oculotoxic drugs using the zebrafish visualmotor response. *J Pharmacol Toxicol Methods* **2014**, *69*, 1-8, doi:10.1016/j.vascn.2013.09.002.

96. Inoue, D.; Wittbrodt, J. One for all--a highly efficient and versatile method for fluorescent immunostaining in fish embryos. *PLoS One* **2011**, *6*, e19713, doi:10.1371/journal.pone.0019713.

97. Zhang, J.; Zhou, H.; Chen, J.; Lv, X.; Liu, H. Aloperine protects human retinal pigment epithelial cells against hydrogen peroxide-induced oxidative stress and apoptosis through activation of Nrf2/HO-1 pathway. *J Recept Signal Transduct Res* **2022**, *42*, 88-94, doi:10.1080/10799893.2020.1850787.

98. Maeda, T.; Golczak, M.; Maeda, A. Retinal photodamage mediated by all-trans-retinal. *Photochem Photobiol* **2012**, *88*, 1309-1319, doi:10.1111/j.1751-1097.2012.01143.x.

99. Meng, T.; Kulkarni, V.; Simmers, R.; Brar, V.; Xu, Q. Therapeutic implications of nanomedicine for ocular drug delivery. *Drug Discov Today* **2019**, *24*, 1524-1538, doi:10.1016/j.drudis.2019.05.006.

100. Berillo, D.; Zharkinbekov, Z.; Kim, Y.; Raziyeva, K.; Temirkhanova, K.; Saparov, A. Stimuli-Responsive Polymers for Transdermal, Transmucosal and Ocular Drug Delivery. *Pharmaceutics* **2021**, *13*, doi:10.3390/pharmaceutics13122050.

101. Eftimiadi, G.; Soligo, M.; Manni, L.; Di Giuda, D.; Calcagni, M.L.; Chiaretti, A. Topical delivery of nerve growth factor for treatment of ocular and brain disorders. *Neural Regen Res* **2021**, *16*, 1740-1750, doi:10.4103/1673-5374.306062.

102. Brastrom, L.K.; Scott, C.A.; Dawson, D.V.; Slusarski, D.C. A High-Throughput Assay for Congenital and Age-Related Eye Diseases in Zebrafish. *Biomedicines* **2019**, *7*, doi:10.3390/biomedicines7020028.

103. Blanks, J.C.; Johnson, L.V. Specific binding of peanut lectin to a class of retinal photoreceptor cells. A species comparison. *Invest Ophthalmol Vis Sci* **1984**, *25*, 546-557.

104. Cao, G.F.; Liu, Y.; Yang, W.; Wan, J.; Yao, J.; Wan, Y.; Jiang, Q. Rapamycin sensitive mTOR activation mediates nerve growth factor (NGF) induced cell migration and pro-survival effects against hydrogen peroxide in retinal pigment epithelial cells. *Biochem Biophys Res Commun* **2011**, *414*, 499-505, doi:10.1016/j.bbrc.2011.09.094.

105. Cheng, A.C.; Pang, C.P.; Leung, A.T.; Chua, J.K.; Fan, D.S.; Lam, D.S. The association between cigarette smoking and ocular diseases. *Hong Kong Med J* **2000**, *6*, 195-202.

106. Chen, Y.; Okano, K.; Maeda, T.; Chauhan, V.; Golczak, M.; Maeda, A.; Palczewski, K. Mechanism of all-trans-retinal toxicity with implications for stargardt disease and age-

related macular degeneration. *J Biol Chem* **2012**, *287*, 5059-5069, doi:10.1074/jbc.M111.315432.

107. Velilla, S.; García-Medina, J.J.; García-Layana, A.; Dolz-Marco, R.; Pons-Vázquez, S.; Pinazo-Durán, M.D.; Gómez-Ulla, F.; Arévalo, J.F.; Díaz-Llopis, M.; Gallego-Pinazo, R. Smoking and age-related macular degeneration: review and update. *J Ophthalmol* **2013**, *2013*, 895147, doi:10.1155/2013/895147.
108. Kunchithapautham, K.; Atkinson, C.; Rohrer, B. Smoke exposure causes endoplasmic reticulum stress and lipid accumulation in retinal pigment epithelium through oxidative stress and complement activation. *J Biol Chem* **2014**, *289*, 14534-14546, doi:10.1074/jbc.M114.564674.
109. Bertram, K.M.; Baglole, C.J.; Phipps, R.P.; Libby, R.T. Molecular regulation of cigarette smoke induced-oxidative stress in human retinal pigment epithelial cells: implications for age-related macular degeneration. *Am J Physiol Cell Physiol* **2009**, *297*, C1200-1210, doi:10.1152/ajpcell.00126.2009.
110. Espinosa-Heidmann, D.G.; Suner, I.J.; Catanuto, P.; Hernandez, E.P.; Marin-Castano, M.E.; Cousins, S.W. Cigarette smoke-related oxidants and the development of sub-RPE deposits in an experimental animal model of dry AMD. *Invest Ophthalmol Vis Sci* **2006**, *47*, 729-737, doi:10.1167/iovs.05-0719.
111. Suñer, I.J.; Espinosa-Heidmann, D.G.; Marin-Castano, M.E.; Hernandez, E.P.; Pereira-Simon, S.; Cousins, S.W. Nicotine increases size and severity of experimental choroidal neovascularization. *Invest Ophthalmol Vis Sci* **2004**, *45*, 311-317, doi:10.1167/iovs.03-0733.
112. Fujihara, M.; Nagai, N.; Sussan, T.E.; Biswal, S.; Handa, J.T. Chronic cigarette smoke causes oxidative damage and apoptosis to retinal pigmented epithelial cells in mice. *PLoS One* **2008**, *3*, e3119, doi:10.1371/journal.pone.0003119.
113. Massarsky, A.; Jayasundara, N.; Bailey, J.M.; Oliveri, A.N.; Levin, E.D.; Prasad, G.L.; Di Giulio, R.T. Teratogenic, bioenergetic, and behavioral effects of exposure to total particulate matter on early development of zebrafish (Danio rerio) are not mimicked by nicotine. *Neurotoxicol Teratol* **2015**, *51*, 77-88, doi:10.1016/j.ntt.2015.09.006.
114. Ellis, L.D.; Soo, E.C.; Achenbach, J.C.; Morash, M.G.; Soanes, K.H. Use of the zebrafish larvae as a model to study cigarette smoke condensate toxicity. *PLoS One* **2014**, *9*, e115305, doi:10.1371/journal.pone.0115305.
115. de Haan, J.B.; Bladier, C.; Griffiths, P.; Kelner, M.; O'Shea, R.D.; Cheung, N.S.; Bronson, R.T.; Silvestro, M.J.; Wild, S.; Zheng, S.S.; et al. Mice with a homozygous null mutation for the most abundant glutathione peroxidase, Gpx1, show increased susceptibility to the

oxidative stress-inducing agents paraquat and hydrogen peroxide. *J Biol Chem* **1998**, *273*, 22528-22536, doi:10.1074/jbc.273.35.22528.

116. Duong, C.; Seow, H.J.; Bozinovski, S.; Crack, P.J.; Anderson, G.P.; Vlahos, R. Glutathione peroxidase-1 protects against cigarette smoke-induced lung inflammation in mice. *Am J Physiol Lung Cell Mol Physiol* **2010**, *299*, L425-433, doi:10.1152/ajplung.00038.2010.
117. Timme-Laragy, A.R.; Van Tiem, L.A.; Linney, E.A.; Di Giulio, R.T. Antioxidant responses and NRF2 in synergistic developmental toxicity of PAHs in zebrafish. *Toxicol Sci* **2009**, *109*, 217-227, doi:10.1093/toxsci/kfp038.
118. Zhang, L.; Zhou, Y.; Xia, Q.; Chen, Y.; Li, J. All-trans-retinal induces autophagic cell death via oxidative stress and the endoplasmic reticulum stress pathway in human retinal pigment epithelial cells. *Toxicol Lett* **2020**, *322*, 77-86, doi:10.1016/j.toxlet.2020.01.005.
119. Chen, C.; Yang, K.; He, D.; Yang, B.; Tao, L.; Chen, J.; Wu, Y. Induction of ferroptosis by HO-1 contributes to retinal degeneration in mice with defective clearance of all-trans-retinal. *Free Radic Biol Med* **2023**, *194*, 245-254, doi:10.1016/j.freeradbiomed.2022.12.008.
120. Li, J.; Cai, X.; Xia, Q.; Yao, K.; Chen, J.; Zhang, Y.; Naranmandura, H.; Liu, X.; Wu, Y. Involvement of endoplasmic reticulum stress in all-trans-retinal-induced retinal pigment epithelium degeneration. *Toxicol Sci* **2015**, *143*, 196-208, doi:10.1093/toxsci/kfu223.
121. Li, S.; Sato, K.; Gordon, W.C.; Sendtner, M.; Bazan, N.G.; Jin, M. Ciliary neurotrophic factor (CNTF) protects retinal cone and rod photoreceptors by suppressing excessive formation of the visual pigments. *J Biol Chem* **2018**, *293*, 15256-15268, doi:10.1074/jbc.RA118.004008.
122. Cocchiaro, P.; Di Donato, V.; Rubbini, D.; Mastropasqua, R.; Allegretti, M.; Mantelli, F.; Aramini, A.; Brandolini, L. Intravitreal Administration of rhNGF Enhances Regenerative Processes in a Zebrafish Model of Retinal Degeneration. *Front Pharmacol* **2022**, *13*, 822359, doi:10.3389/fphar.2022.822359.
123. Gong, Y.; He, X.; Li, Q.; He, J.; Bian, B.; Li, Y.; Ge, L.; Zeng, Y.; Xu, H.; Yin, Z.Q. SCF/SCFR signaling plays an important role in the early morphogenesis and neurogenesis of human embryonic neural retina. *Development* **2019**, *146*, doi:10.1242/dev.174409.
124. Jeon, S.; Oh, I.H. Regeneration of the retina: toward stem cell therapy for degenerative retinal diseases. *BMB Rep* **2015**, *48*, 193-199, doi:10.5483/bmbrep.2015.48.4.276.

LIST OF PUBLICATIONS

- Piano, I.; Votta, A.; **Colucci, P.**; Corsi, F.; Vitolo, S.; Cerri, C.; Puppi, D.; Lai, M.; Maya-Vetencourt, J.F.; Leigheb, M.; Gabellini, C.; Ferraro, E. Anti-inflammatory reprogramming of microglia cells by metabolic modulators to counteract neurodegeneration; a new role for Ranolazine. *Manuscript submitted in Scientific Report.*

- Gómez Sánchez, A.; **Colucci, P.**; Moran, A.; Moya López, A.; Colligris, B.; Álvarez, Y.; Kennedy, B.N. Systemic Treatment with Cigarette Smoke Extract Affects Zebrafish Visual Behaviour, Intraocular Vasculature Morphology and Outer Segment Phagocytosis. *Manuscript under review in Open Research Europe.*

- **Colucci, P.**; Giannaccini, M.; Baggiani, M.; Kennedy, B.N.; Dente, L.; Raffa, V.; Gabellini, C. Neuroprotective nanoparticles targeting the retina: a polymeric platform for ocular drug delivery applications. *Pharmaceutics, 2023, 15(4):1096..*

- **Colucci, P.**; Damora, M.; Usai, A.; Landi, E.; Deleye, L.; Dente, L.; De Angelis, F.; Raffa, V.; Tantussi, F. Heat-sensitive poly-acrylamide nanoparticle for cancer treatment. *Precision Nanomedicine, 2020, 3(5):666-676.*

- Usai, A.; Di Franco, G.; **Colucci, P.**; Pollina, L.E.; Vasile, E.; Funel, N.; Palmeri, M.; Dente, L.; Falcone, A.; Morelli, L.; Raffa, V. A Model of a Zebrafish Avatar for Co-Clinical Trials. *Cancers, 2020, 12(3), 677.*

CONTRIBUTIONS TO INTERNATIONAL CONFERENCES

- **Retina 2022 Conference**

  Colucci, P.; Dente, L.; Gabellini C.; Raffa, V.; Kennedy, B.N. Pharmacological modulation of zebrafish visual behaviour using all-*trans* retinal and cigarette smoke extract. 3-5th November 2022, Dublin, Ireland (Poster).

- **NanoMed 2022 International Conference and Exhibition**

  Colucci, P.; Dente, L.; Raffa, V.; Gabellini C. Neuroprotective Peanut Agglutinin-Targeted Nanoparticles for Ocular Drug Delivery Applications. 26- 28th October 2022, Athens, Greece (Oral presentation).

- **5th BraYn Conference**

  Colucci, P.; Giuseppetti, G.; Dente, L.; Raffa, V.; Gabellini, C. Therapeutic potential of nanoformulations in a zebrafish model of retinal degeneration. 28 – 30th September 2022, Rome, Italy (Poster).

- **Virtual 11th European Zebrafish Meeting**

  Colucci, P.; Damora, M.; Usai, A.; Landi, E.; Deleye, L.; Dente, L.; De Angelis, F.; Tantussi, F.; Raffa, V. Heat-sensitive polyacrylamide nanoparticle for cancer treatment. 26 – 27th October 2020 (Poster).